THE JOURNAL OF BIOLOGICAL CHEMISTRY VOL. 288, NO. 20, pp. 14341–14361, May 17, 2013
Published in the U.S.A.

Salivary Antigen-5/CAP Family Members Are Cu^{2+}-dependent Antioxidant Enzymes That Scavenge $O_2^{\cdot-}$ and Inhibit Collagen-induced Platelet Aggregation and Neutrophil Oxidative Burst*

Received for publication, March 5, 2013, and in revised form, April 4, 2013 Published, JBC Papers in Press, April 5, 2013, DOI 10.1074/jbc.M113.466995

Teresa C. F. Assumpção[‡], Dongying Ma[‡], Alexandra Schwarz[§1], Karine Reiter[¶], Jaime M. Santana[‖], John F. Andersen[‡], José M. C. Ribeiro[‡], Glenn Nardone[**], Lee L. Yu[‡‡], and Ivo M. B. Francischetti[‡2]

From the [‡]Vector Biology Section, Laboratory of Malaria and Vector Research, NIAID, National Institutes of Health, Bethesda, Maryland, 20892, the [§]Institute of Parasitology, Academy of Sciences of the Czech Republic, Biology Centre, 37005 Ceske Budejovice, Czech Republic, the [¶]Laboratory of Malaria Immunology and Vaccinology, NIAID, National Institutes of Health, Rockville, Maryland 20852, the [‖]Pathogen-Host Interface Laboratory, Department of Cell Biology, University of Brasília, 70910-900 Brasília, Brazil, the [**]Research Technology Branch, NIAID, National Institutes of Health, Rockville, Maryland 20852, and the [‡‡]Chemical Sciences Division, National Institute of Standards and Technology, Gaithersburg, Maryland 20899-8391

Background: The function of most salivary antigen-5/CAP members has remained elusive for decades.
Results: Antigen-5 members bind Cu^{2+} and exhibit antioxidant activity by scavenging $O_2^{\cdot-}$. It inhibits platelet aggregation by collagen and neutrophil oxidative burst.
Conclusion: Antigen-5 emerges as a novel family of antioxidant enzymes targeting $O_2^{\cdot-}$.
Significance: Scavenging $O_2^{\cdot-}$ is conceivably associated with decreased inflammation in the microcirculation and may assist blood-sucking insects to successfully feed on blood.

The function of the antigen-5/CAP family of proteins found in the salivary gland of bloodsucking animals has remained elusive for decades. Antigen-5 members from the hematophagous insects *Dipetalogaster maxima* (DMAV) and *Triatoma infestans* (TIAV) were expressed and discovered to attenuate platelet aggregation, ATP secretion, and thromboxane A_2 generation by low doses of collagen (<1 μg/ml) but no other agonists. DMAV did not interact with collagen, glycoprotein VI, or integrin $\alpha 2\beta 1$. This inhibitory profile resembles the effects of antioxidants Cu,Zn-superoxide dismutase (Cu,Zn-SOD) in platelet function. Accordingly, DMAV was found to inhibit cytochrome *c* reduction by $O_2^{\cdot-}$ generated by the xanthine/xanthine oxidase, implying that it exhibits antioxidant activity. Moreover, our results demonstrate that DMAV blunts the luminescence signal of $O_2^{\cdot-}$ generated by phorbol 12-myristate 13-acetate-stimulated neutrophils. Mechanistically, inductively coupled plasma mass spectrometry and fluorescence spectroscopy revealed that DMAV, like Cu,Zn-SOD, interacts with Cu^{2+}, which provides redox potential for catalytic removal of $O_2^{\cdot-}$. Notably, surface plasmon resonance experiments (BIAcore) determined that DMAV binds sulfated glycosaminoglycans (*e.g.* heparin, K_D ~100 nmol/liter), as reported for extracellular SOD. Finally, fractions of the salivary gland of *D. maxima* with native DMAV contain Cu^{2+} and display metal-dependent antioxidant properties. Antigen-5/CAP emerges as novel family of Cu^{2+}-dependent antioxidant enzymes that inhibit neutrophil oxidative burst and negatively modulate platelet aggregation by a unique salivary mechanism.

The presence of anti-hemostatics in the salivary glands (SGs)[3] of hematophagous animals is an evolutionary strategy aimed to decrease the inflammatory tonus that emerges at sites of insect bite (1). These responses comprise a series of complex biochemical reactions that ultimately prevent blood loss. In this respect, several anticoagulants, platelet inhibitors, and vasodilators have been identified in most salivary secretions studied to date (1). Notably, a remarkable diversity of mechanisms accounts for the anti-hemostatic properties of saliva. For example, platelet aggregation is blocked by apyrases or ADP-, TXA_2-, or serotonin-binding proteins; collagen inhibitors; integrin $\alpha_2\beta_1$ or $\alpha_{IIb}\beta_3$ antagonists; cAMP or cGMP intraplatelet-in-

* This work was supported, in whole or in part, by National Institutes of Health Grant ZIA AI000810-16 and by the Intramural Research Program of the Division of Intramural Research, NIAID, National Institutes of Health. This work was also supported by and Brazilian grants from Fundacao de Amparo à Pesquisa do Distrito Federal, Conselho Nacional de Desenvolvimento Cientifico e Tecnológico, and Financiadora de Estudos e Projetos.
[1] Supported by Grant Agency of the Czech Republic Grant P302/11/P798 and Ministry of Education, Youth, and Sports of the Czech Republic KONTAKT II Grant LH12002.
[2] To whom correspondence should be addressed: Laboratory of Malaria and Vector Research, NIAID, National Institutes of Health, 12735 Twinbrook Pkwy., Rm. 2E-32C, Bethesda, MD 20852. Tel.: 301-402-2748; Fax: 301-480-2571; E-mail: ifrancischetti@niaid.nih.gov.

[3] The abbreviations used are: SG, salivary gland; SGH, salivary gland homogenate; DMAV, *D. maxima* antigen-5; TIAV, *T. infestans* antigen-5; SOD, superoxide dismutase; MnTMPyP, manganese(III) tetrakis(1-methyl-4-pyridyl)-porphyrin; ROS, reactive oxygen species; GPVI, glycoprotein VI; TXA_2 and TXB_2, thromboxane A_2 and B_2, respectively; PAF, platelet-activating factor; SEC, size exclusion chromatography; MALS, multiangle light scattering; QELS, quasi-elastic light scatter detection; X/XO, xanthine/xanthine oxidase; HBSS, Hanks' buffered saline solution; cyt *c*, cytochrome *c*; PMA, phorbol 12-myristate 13-acetate; ICP-MS, inductively coupled plasma mass spectrometry; ITC, isothermal titration calorimetry; SPR, surface plasmon resonance; RU, response unit(s); PC/PS, phosphatidylserine/phosphatidylcholine; DS50K, 50,000-Da dextran sulfate; DS500K, 500,000-Da dextran sulfate; Cvx, convulxin.

creasing molecules (PGI_2, adenosine, and NO); anti-thrombins; and fibrin(ogen)olytic enzymes (2).

Although the anti-hemostatic functions of several molecules in SGs are mediated by well known family of proteins, such as serpins, lipocalins, apyrases, and kazal and kunitz domain-containing molecules, several other inhibitors of platelet aggregation or coagulation cascade have not been characterized molecularly. More recently, transcriptome and proteome analysis (sialomes) of numerous SGs from hematophagous sources revealed that this tissue is a source of an unprecedented number of uniquely expressed proteins (*e.g.* 30-kDa allergens, yellow proteins, and antigen-5) (1, 3). Most often, the biological functions for members of these families have not been assigned. Notably, antigen-5 members, which belong to the CAP superfamily (cysteine-rich secretory proteins, antigen 5, and pathogenesis-related 1 proteins) of proteins, is inarguably one of the most, if not the most, ubiquitous family of salivary proteins, together with apyrases (3). The function of this family has remained elusive despite its presence in mosquitoes, sand flies, bugs, horse flies, Culicidae, Simulidae, ticks, and venomous animals (1). Only one salivary antigen-5 member has been unambiguously identified as an RGD-containing disintegrin by incorporation of a typical RGD triad flanked by cysteines not found in other antigen-5 members (4, 5).

In our attempt to identify the function of this family of proteins, we discovered that antigen-5 members from the SG of the *Triatomine* vectors of Chagas disease, *Dipetalogaster maxima* (DMAV, *D. maxima* antigen-5) (6) and *Triatoma infestans* (TIAV, *T. infestans* antigen-5) (7) were inhibitors of low doses of collagen-induced platelet aggregation. DMAV did not interfere with aggregation triggered by other agonists or block the proximal interaction of collagen with platelets. This inhibitory profile resembles the inhibitory effects of antioxidants in platelet aggregation induced by collagen, which is the only agonist-promoting extracellular increase of $O_2^{\cdot-}$ (8–11), in addition to intracellular reactive oxygen species (ROS). For example, blockade of extracellular $O_2^{\cdot-}$ by *N*-acetylcysteine is accompanied by inhibition of low doses of collagen-induced platelet aggregation (12). In addition, Zn,Cu-SOD prevents platelet recruitment induced by collagen *in vitro* (10).

While the interplay of collagen and ROS has long been recognized (13–23), only more recently has it been explained molecularly (8, 9). Collagen interacts with GPVI, which signals by tyrosyl phosphorylation and NADPH oxidase activation through TRAF4 (24). These steps result in the generation of $O_2^{\cdot-}$ that is critical to prime the cyclo-oxygenase enzyme for kinase activation (13, 24). Accordingly, intracellular $O_2^{\cdot-}$ is important for collagen-induced platelet activation. NADPH oxidase inhibitor apocynin (12) or intracellular antioxidants, such as MnTMPyP, inhibit intracellular ROS formation by collagen and attenuate TXB_2 production and platelet aggregation (20). Furthermore, quercetin, which displays antioxidant properties, attenuates platelet aggregation by collagen (25).

Mechanistically, it was found that DMAV binds Cu^{2+} and catalytically removes $O_2^{\cdot-}$. Therefore, this report is the first to determine the function of the antigen-5 family of salivary proteins as antioxidant enzymes. This discovery is important, given the wide expression of antigen-5 family members in bloodsucking animals, venomous creatures, and vertebrates (26). It also highlights the importance of scavenging $O_2^{\cdot-}$ to attenuate the proinflammatory events associated with dysregulated production of ROS in the microcirculation.

EXPERIMENTAL PROCEDURES

Materials—Horse tendon insoluble Horm fibrillar collagen was from Chrono-Log Corp. (Haverstown, PA). Soluble collagen type I was from BD Biosciences. PGD_2, PGE_2, $PGF_{2\alpha,\ PGG2}$, PGH_2 endoperoxide mimetic (U-51605), PGJ_2, $cTXA_2$, TXA_2 mimetic (U-46619), TXB_2, LTC_4, 5(*S*)-HETE, 9(*S*)-HETE, 15(*S*)-HETE, and 20-HETE were obtained from Cayman Chemicals (Ann Arbor, MI). ADP, norepinephrine, epinephrine, serotonin, indomethacin, PAF, and histamine were purchased from Sigma. Sensor CM5, amine-coupling reagents, and buffers were purchased from GE Healthcare. Heparin grade I-A from porcine intestinal mucosa (average molar mass 17–19 kDa; H3149), heparin grade II from porcine intestinal mucosa (H7005), heparan sulfate from bovine kidney (average molar mass 10–12 kDa; H7640), chondroitin sulfate C from shark cartilage (molar mass 50 kDa; C4384), dextran sulfate sodium from *Leuconostoc* spp. (average molar mass 9–20 kDa; D6924), dextran sulfate 50K (Dextralip50) (average molar mass 50 kDa; D-8787), dextran sulfate 500K from *Leuconostoc* spp. (average molar mass >500 kDa; D8906), lucigenin (*N*,*N*′-dimethyl-9,9′-biacridinium dinitrate), luminol (3-aminophthalhydrazide, 5-amino-2,3-dihydro-1,4-phthalazinedione), cytochrome *c* from bovine heart (C3131), hypoxanthine (6-hydroxypurine; H-9377), xanthine oxidase (Grade III, 1–2 units/mg protein; 1.4 units/mg protein; 14 units/ml) from bovine milk (X4500), and Cu,Zn-SOD from bovine liver (S8409; 4,800 units/mg; 9,600 units/ml) were purchased from Sigma. Dextran (non-sulfated) standard 670 kDa (00896) and dextran (non-sulfated) standard 12 kDa (00270) were from Biochemika (Steinheim, Denmark). Enoxaparin (4,500 Da; 100 mg/ml) was from Sandoz (Princeton, NJ). Convulxin was purified as described (27), and GPVI was expressed as reported (28).

Sequence Analysis—Sequence similarity searches were performed using BLAST. Cleavage site predictions of the mature proteins used the SignalP program. The molar extinction coefficient ($\epsilon_{280\ nm}$) of mature DMAV (gi 344190589) at 280 nm was obtained using the ProtParam Web site, yielding a value of $\epsilon_{280\ nm}$ = 58,705 mol liter^{-1}·cm^{-1} $A_{0.1\%}^{280\ nm}$/cm (1 mg/ml) = 1.217, predicted molar mass 25,341 Da (224 amino acids), and isoelectric point (pI) 8.57.

Clustal Alignment and Phylogenetic Tree Construction—A sequence similarity search to DMAV was performed using protein BLAST against Arthropoda organisms with a low complexity region filter. The sequences derived from the nonredundant protein database of the National Center for Biotechnology Information (NCBI) are represented by five letters followed by the NCBI gi accession number. The five letters derive from the first three letters of the genus and the first two letters from the species name. The protein sequences were aligned by the ClustalX software program. The phylogenetic tree was created with the Mega package after 10,000 bootstraps with the neighbor-joining algorithm, using the *p*-dis-

tance model as described (6, 29). The bar at the bottom of each tree represents 10% amino acid substitution.

Expression of DMAV and TIAV in Escherichia coli—All percentage concentrations are expressed as the volume fraction of the chemical in water. Synthetic cDNA for DMAV (gi 344190589) was produced by BioBasic Inc. (Markham, Canada). The sequence displays an N-terminal NdeI and a C-terminal XhoI restriction site. The NdeI site adds a 5′-methionine codon to all sequences that acts as start codon in the bacterial expression system, whereas the XhoI site was incorporated after a stop codon. pET17b constructs were confirmed by sequencing before transformation by heat shock of *E. coli* strain BL21(DE3)pLysS cells. Cells were grown overnight in LB ampicillin/chloramphenicol agar plates, at 37 °C. Colonies were picked and then used to generate glycerol stocks (25% volume fraction). For recombinant protein production, a protocol similar to that described was employed (30). Briefly, 30 ml of Luria-Bertani broth (with 34 μg/ml chloramphenicol and 100 μg/ml ampicillin) was inoculated and grown overnight for a maximum of 16 h at 37 °C. Luria-Bertani broth (1 liter with 34 μg/ml chloramphenicol and 100 μg/ml ampicillin) was inoculated with 10 ml of the overnight culture and grown at 37 °C with continuous shaking (26 rads/s) until an optical density of 0.6–0.8 ($A_{600\ nm}$) was reached (~3 h). Isopropyl-1-thio-β-D-galactopypyranoside (1 mmol/liter) was added to induce expression, and the flask was shaken for 3 h under the same conditions; cells were harvested by centrifugation (6,000 × g_n; 20 min) and washed once in 20 mmol/liter Tris-HCl, pH 8.0, before the cell pellet was frozen and stored until use. Pellets were sonicated several times, washed in 20 mmol/liter Tris, pH 8.3, centrifuged, and finally resuspended in 25 ml of 20 mmol/liter Tris, pH 8.3, containing 6 M guanidine and DTT (10 mmol/liter). After 1 h, the sample was centrifuged at 16,000 × g for 30 min. Twenty-five ml was added slowly, drop-by-drop, into 4 liters of refolding buffer (20 mmol/liter Tris, 0.3 mol/liter arginine, 1 mmol/liter EDTA, 1 mmol/liter reduced glutathione (GSH), and 0.2 mmol/liter oxidized glutathione (GSSG), pH 9.3) under agitation. After 2 days under agitation at 4 °C, the solution containing DMAV was concentrated to ~300 ml by tangential flow with a 10-kDa cut-off filter (Millipore, Inc., Billerica, MA). Sample was centrifuged (12,000 × g_n for 20 min) and concentrated to 30 ml in a Millipore ultrafiltration apparatus (membrane of 10 kDa). The sample was centrifuged (12,000 × g_n for 20 min), and the supernatant was used for protein purification (see below). Antigen-5 members from *T. infestans* (gi 149898844) were cloned in pET17b and expressed as above except that refolding was performed at pH 7.4. As a control, a lipocalin from *D. maxima* (DM146, gi 315270899) was cloned, expressed, and purified as above.

Protein Purification—DMAV (10 ml) was loaded into a HiPrep 16/60 Sephacryl S-100 HR (GE Healthcare) column connected to an AKTA purifier system (Amersham Biosciences) and equilibrated in 20 mmol/liter Tris-HCl, 0.15 mol/liter NaCl, pH 9.3, with a flow of 1 ml/min. Protein was detected by peak absorbance at 280 and 220 nm, and fractions containing DMAV (estimated by SDS-PAGE) were combined (4 ml) and concentrated in a Centricon concentrator (10 kDa cut-off). Samples were loaded in a gel filtration column (Superdex 75 HR10/30, Amersham Biosciences) equilibrated in 20 mmol/liter Tris-HCl, 0.5 mol/liter NaCl, pH 9.3. Elution was carried out at a flow rate of 1 ml/min, and fractions containing DMAV were combined. Fractions were dialyzed against 20 mmol/liter Tris-HCl and loaded in a Mono Q anion exchange column (Amersham Biosciences). To remove bacterial DNA potentially contaminating DMAV, the fractions containing DMAV were combined and dialyzed against 10 mmol/liter HEPES, pH 6.0, centrifuged, and loaded into cation exchange chromatography using a HiPrep 16/10 SP FF column (Amersham Biosciences). Proteins were eluted with a linear gradient of NaCl (0–1 mol/liter) over 60 min at a flow rate of 0.5 ml/min. Fractions containing DMAV were combined and dialyzed against PBS, pH 7.4. DMAV was also purified in a reversed-phase C-18 chromatography column (Vydac, Carpenteria, CA), with a 60-min linear gradient of acetonitrile and 0.1% TFA at a flow rate of 1 ml/min. PAGE and Edman degradation were performed as described (30).

Mass Spectrometry of Purified DMAV—DMAV molecular weight was determined with a Sciex 4000 Q Trap ESI mass spectrometer.

Circular Dichroism—To examine secondary structure, samples were diluted in 1× PBS. CD spectra were recorded over the wavelength range 190–260 nm in a 1-mm path length quartz cuvette using a step size of 0.2 nm, a slit bandwidth of 1.0 nm, and a signal averaging time of 1.0 s using a Jasco J-815 circular dichroism spectrometer. Percentages of secondary structures were determined as described (31, 32).

SEC-MALS-QELS-HPLC—To assess the identity, purity, and solution aggregation state of purified DMAV (17 μmol/liter), analytical size exclusion chromatography (SEC) with in-line multiangle light scattering (MALS) and quasi-elastic light scatter detection (QELS) was performed. Chromatography was done on an Alliance HPLC system (Waters Corp., Milford MA) connected to a multiangle DAWN EOS MALS detector and a QELS detector (Wyatt Technology, Santa Barbara, CA).

Spectrum of DMAV—Spectrum of DMAV (500 μl at 5 μmol/liter in TBS, pH 7.4) was analyzed by UV-visible spectroscopy wavelength scanning (Cary 100 BIO spectrophotometer; Varian Inc., Walnut Creek, CA) using the eluent buffer (TBS) as a blank. Aliquots of $CuCl_2$ (in TBS, pH 7.4) were added in 10-μl increments, reaching a maximum concentration of 100 μmol/liter $CuSO_4$.

Determination of Free Cysteine in DMAV—Reactions for thiol modification were done at room temperature in 100 μl of 20 mmol/liter Tris-HCl, pH 8.0, 1 mmol/liter 4-fluoro-7-aminosulfonylbenzofurazan, 20% DMSO for 1 h. The reactions were read in a Tecan M200 plate reader at excitation and emission wavelengths of 386 and 516 nm, respectively. Reduction of DMAV was done with 10 mmol/liter TCEP at 40 °C for 20 min. Non-reducing protein denaturation was done in 0.1% volume fraction SDS at 60 °C for 30 min. In some experiments, DMAV was incubated with buffer or xanthine/xanthine oxidase (X/XO) followed by mass spectrometry (MS).

Anti-DMAV Polyclonal Antibody—Recombinant DMAV produced in *E. coli* was diluted to 1 mg/ml and injected in the presence of Freund's adjuvant in rabbits at Spring Valley Laboratories (Woodbine, MD). Additional injections were per-

formed 3, 6, and 9 weeks later to boost the immune response. Before injection of DMAV, preimmune serum was obtained from all rabbits.

ELISA to Detect DMAV—Antibody titer was estimated by ELISA using bacterial expressed DMAV (0.5 μg/well) immobilized overnight in PBS at 4 °C. Wells were blocked with 200 μl of TBS-BSA (BSA (2%, w/v) in TBS) for 2 h and then incubated for 1 h with a serial dilution of anti-DMAV antibody in TBS-BSA-Tween (BSA, 1% volume fraction; Tween, 0.05% volume fraction in TBS). After washing four times with TBS-BSA-Tween, the wells were incubated with a 1:2,000 dilution of anti-rabbit alkaline phosphatase-coupled antibody for 1 h and washed four times with TBS-BSA-Tween. Two hundred μl of substrate (*p*-nitrophenyl phosphate liquid substrate system; Sigma) was added, and reactions were followed for 10 min and stopped with 100 μl of NaOH (0.375 mol/liter, final concentration). Absorbance was detected at 405 nm.

D. maxima Salivary Gland Purification—For some experiments, the supernatant from the homogenate obtained from 50 pairs of *D. maxima* (reared at the Institute of Parasitology, Biology Centre, Ceske Budejovice, Czech Republic) was applied to a Sephadex G-75 column, equilibrated with PBS, pH 7.4, at a flow rate of 0.5 ml/min.

Mass Spectrometry and Protein Identification—Samples from selected fractions obtained above were solubilized in NU/PAGE sample buffer containing DTT and loaded into a 4–12% NuPAGE gel with MES buffer (Invitrogen). The gel was cut in 20 slices of ~0.5 cm (from top to bottom of each lane), and identification was performed on reduced and alkylated, trypsin-digested samples prepared by standard MS protocols. The supernatant and two washes (5% formic acid in 50% acetonitrile) of the gel digests were pooled and concentrated by SpeedVac (Labconco, Kansas City, MO) to dryness directly in 200 μl of polypropylene autosampler vials (Sun Sri, Rockwood, TN). Recovered peptides were resuspended in 5 μl of solvent A (0.1% formic acid, 2% acetonitrile, and 97.9% water).

Prior to MS analysis, the resuspended peptides were chromatographed directly on the column without trap clean-up. Bound peptides were separated at 500 nl/min, generating 80–120 bar pressure using an AQ C18 reversed-phase medium (3-μm particle size and 200-μm pore) packed in a pulled-tip, nanochromatography column (0.100-mm inner diameter × 150-mm length; Precision Capillary Columns (San Clemente, CA)). Chromatography was performed in-line with an LTQ-Velos Orbitrap mass spectrometer (Thermo Fisher Scientific), and the mobile phase consisted of a linear gradient prepared from solvent A and solvent B (0.1% formic acid, 2% water, and 97.9% acetonitrile) at room temperature. Nano-LC-MS (LC-MS/MS) was performed with a ProXeon Easy-nLC II multidimensional liquid chromatograph and temperature-controlled Ion Max nanospray source (Thermo Fisher Scientific) in-line with the LTQ-Velos Orbitrap mass spectrometer.

Computer-controlled data-dependent automated switching to MS/MS by Xcalibur version 2.1 software was used for data acquisition and provided the peptide sequence information. Data processing and data bank searching were performed with Proteome Discoverer version 1.2 and SEQUEST (Thermo Scientific). The data were searched against protein sequences in the database generated with the salivary gland of *D. maxima* (6). Parsimony analysis was performed using ProteoIQ software (NuSep, Athens, GA), and protein probabilities were calculated using the ProteinProphet algorithm. All proteins were required to have at least two peptides and two spectra per peptide and a probability of 95% in at least one gel lane. MS/MS results were mapped into the Excel spreadsheet with indication of the slices containing the most abundant ions in sorted order, among other information.

Platelet Preparation, Aggregation, ATP Secretion, and TXA_2 Generation—Platelet-rich plasma was obtained under informed consent from medication-free platelet donors participating in a National Institutes of Health Institutional Review Board-approved protocol of the Department of Transfusion Medicine (DTM/NIH, Blood Bank). Platelet-rich plasma (100 μl) was added to 200 μl of Tyrode's buffer (137 mmol/liter NaCl, 27 mmol/liter KCl, 12 mmol/liter $NaHCO_3$, 0.42 mmol/liter NaH_2PO_4, 1 mmol/liter $MgCl_2$, 5.55 mmol/liter Hepes, 0.25% bovine serum albumin, pH 7.4) giving a final concentration of 200,000–400,000 platelets/μl. Platelet aggregation was estimated using a Lumi-Aggregometer (Chrono-Log Corp.) under agitation as reported (30). In experiments using PGG_2, platelets were washed and resuspended in Tyrode's buffer supplemented with gelatin (0.25% volume fraction). PAF was prepared as described (30). To estimate dense granule ATP release, peak luminescence was detected by adding luciferin-luciferase (20 μl) 4 min after the addition of collagen. For TXA_2 generation, platelets were activated by collagen, and after 4 min, the sample was transferred to an Eppendorf tube and centrifuged for 15 s at 14,000 × g_n. The supernatant was immediately frozen in dry ice, and then at −80 °C. The next day, the sample was thawed and used at a 1:300 dilution for detection of TXB_2 by competitive ELISA (Cayman).

Platelet Adhesion—For platelet adhesion assays, platelet-rich plasma was incubated with calcein-AM (2 μmol/liter, Calbiochem) for 30 min at room temperature and centrifuged in the presence of EDTA (5 mmol/liter) and apyrase (0.2 units/ml). Platelets were resuspended ($2 \times 10^5/\mu$l) in Tyrode's buffer (no additions). Inhibition of platelet adhesion to immobilized collagen was examined by fluorometry. Microfluor black microtiter 96-well plates (ThermoLabsystems, Franklin, MA) were coated with 50 μl (1 μg/well in PBS) of fibrillar (Horm) or soluble collagen I (BD Biosciences) overnight at 4 °C in PBS, pH 7.4. Wells were washed with PBS and blocked with 2% (w/v) BSA (in PBS). Calcein-labeled platelets ($2 \times 10^5/\mu$l) were incubated with DMAV or EDTA for 20 min, and 50 μl of platelets was added to each well. After 1 h, wells were washed three or four times with Tyrode-BSA, and adhesion was estimated by fluorescence (excitation 485 nm/emission 530 nm).

Thrombus Formation—Thrombus formation under flow was performed essentially as described (4).

Neutrophil Preparation—Polyprep medium (6.5 ml; MP Biomedicals, Solon, OH) was added to a 15-ml Falcon tube. Blood (7 ml, collected in 5 mmol/liter EDTA, final concentration) was carefully layered on the Polyprep medium. The tubes were centrifuged at 209 rads/s (863 × g_n) for 45 min using acceleration and deceleration set at 5, at room temperature. Two rings were observed; the upper ring was discarded, and the lower ring was

collected and transferred to a 50-ml Falcon tube. Then HBSS (Cellgro) (no calcium, no magnesium; 40 ml) was added, and cells were centrifuged again for 10 min at 104 rads/s. When contamination with red blood cells was visible, 1 ml of lysis buffer was added to the tubes for 40–50 s, followed by the addition of HBSS (45 ml) and centrifugation as above. The pellet was resuspended in 3 ml and counted, and concentration was adjusted to 2×10^6/ml in HBSS (no Ca^{2+}, no Mg^{2+}). Cells were kept on ice.

O_2^- Production by Neutrophils—In 96-well Chromalux HB flat bottom white polystyrene microplates for luminescent applications (catalog no. 2010) (Dinex Technologies), neutrophils (50 μl at 1×10^6/ml) were added to wells in the presence of DMAV (0–10 μl), followed by the addition of 50 μl of Diogenes reagent (National Diagnostics, Atlanta, GA) or 50 μl of lucigenin (20 μmol/liter, final concentration) or 50 μl of luminol (500 μmol/liter, final concentration) diluted in HBSS. Then 5–10 μl of PMA (10–20 nmol/liter, final concentrations) was added, and luminescence was read in an LMAX II^{384} Plate Luminometer (Molecular Devices, Sunnyvale, CA). Diogenes reagent was diluted as indicated by the manufacturer, whereas lucigenin (40 mmol/liter) and luminol (500 mmol/liter) were diluted in DMSO followed by extensive vortexing.

Xanthine Oxidase Generation of O_2^- Estimated by Luminol or Lucigenin—Fifty μl of reaction mixture (RM) (100 mmol/liter phosphate buffer, pH 7.8, 500 μmol/liter hypoxanthine, and 500 μmol/liter luminol; final concentrations) was added to the wells, followed by the addition of DMAV (0–10 μl). Reactions started with xanthine oxidase (50 μl, 1:2,500, or 1:5,000 final concentrations; ~5 milliunits/ml) using a multichannel pipette. Plates were immediately read using an LMAX II^{384} Luminometer (Molecular Devices), and integrations of the signal were obtained with Softmax Pro software. Results are expressed as luminescence estimated under the curve. Uric acid formation was estimated by the increase in UV absorbance at 293 nm. Phosphate buffer was prepared by mixing 90 mmol/liter Na_2HPO_4 and 10 mmol/liter NaH_2PO_4.

Reduction of Cytochrome c (cyt c)—In a 96-well flat microplate, 100 μl of RM (0.1 mol/liter phosphate buffer, 0.5 mmol/liter hypoxanthine, and 12.0 μM (0.15 mg/ml) cyt *c*, final concentrations) was added to the wells, followed by the addition of DMAV (0–3 μl). Reactions started by the addition of 10 μl of xanthine oxidase (1:2,500; ~5 milliunits/ml, final concentration). The reduction of cyt *c* was continuously detected at 550 nm using a Thermomax ELISA reader (Molecular Devices). For kinetic experiments, DMAV (10 μmol/liter) was incubated with saturating concentrations (20 μmol/liter) of Cu^{2+} or Zn^{2+}, followed by extensive dialysis against PBS. To calculate the K_{cat} of DMAV for O_2^-, data were transformed as described (33).

Measurement of H_2O_2—Measurement of H_2O_2 was performed using Amplex Red reagent (Invitrogen) as described in the manufacturer's instructions. Briefly, an RM was prepared containing 2.35 ml of Krebs-Ringer phosphate (145 mmol/liter NaCl, 5.7 mmol/liter sodium phosphate, 4.86 mmol/liter KCl, 0.54 mmol/liter $CaCl_2$, 1.22 mmol/liter $MgSO_4$, 5.5 mmol/liter glucose, pH 7.35), 50 μl of Amplex Red (50 μmol/liter), and 100 μl of horseradish peroxidase (HRP; 0.1 unit/ml). Then 50 μl of RM was added to 50 μl of neutrophils (0.5×10^6/ml, final concentrations), followed by the addition of PMA (20 nmol/liter to 40 nmol/liter). When a cell-free system was used, 5 μl of hypoxanthine (500 μmol/liter final concentrations) was added to 50 μl of RM (which was diluted in HBSS), with and without DMAV. Reactions were started by the addition of 50 μl of XO (6.4 milliunits/ml to 12.8 millunits/ml, final concentrations). As a control, Cu,Zn-SOD (0.4 milliunit/ml, final concentration) was tested. Reactions were followed with an excitation of 540 nm and emission of 590 nm using a SpectraMAX Gemini XPS Fluorimeter (Molecular Devices).

Measurement of O_2 Consumption—O_2 consumption was monitored at 25 °C using a Gilson 5/6 oxygraph fitted with a Clark electrode as described (33, 34). The electrode was calibrated for absolute O_2 concentration. Reactants were injected using a long tip into the reaction chamber under continuous agitation with a stir bar placed in the base of the chamber. The RM, in a final volume of 1.5 ml, typically contained 100 mmol/liter phosphate buffer, pH 7.8, 0.5 mmol/liter hypoxanthine, and 0.7 milliunit/ml xanthine oxidase. Consumption of O_2 was characterized by a deflection of the recorder. In some experiments, catalase (333 units/ml) or DMAV (0.5 μM) was added to the chamber.

Inductively Coupled Plasma Mass Spectrometry (ICP-MS)—Aqueous samples from DMAV obtained directly from the last purification step (cation exchange column) were extensively dialyzed (cut-off of 10 kDa, Slide-A-Lyzer, Thermo Scientific) against 5 mM Hepes, pH 7.4, and transferred into a 15-ml autosampler tube. The mass of the sample was weighed on a four-place analytical balance by difference. An aliquot of 5 g of diluent consisted of 1.5% volume fraction. Optima grade nitric acid (HNO_3; Fisher) in water was weighed into the tube. The diluted sample was thoroughly mixed by gentle shaking. The contents of the samples were analyzed using the SemiQuant mode of Agilent (Santa Clara, CA) model 7500cs inductively coupled plasma mass spectrometer. The sample introduction system of the mass spectrometer consisted of a PFA microflow (0.1 ml/min) concentric nebulizer, a PFA Scott type double-pass spray chamber, and a sapphire injector. The SemiQuant mode is capable of quantifying elements of the entire periodic table by using the spectral information of the elements. The instrument was calibrated using a solution containing 20 $\mu g\,kg^{-1}$ each of 31 elements (lithium, beryllium, boron, sodium, magnesium, aluminum, calcium, scandium, vanadium, chromium, manganese, cobalt, nickel, copper, zinc, arsenic, selenium, strontium, molybdenum, silver, cadmium, antimony, barium, lanthanum, europium, holmium, ytterbium, thalium, lead, thorium, and uranium) prepared by diluting catalog no. ICP-MSCS ICP-MS calibration standard (High Purity Standards, Charleston, SC) with 1.5% HNO_3. National Institute of Standards and Technology Standard Reference Material (SRM) 1643e, Trace Elements in Water, was measured with the samples. SRM 1643e served as the quality assurance for the measurement (35).

Reconstitution of DMAV with Divalent Ions and Detection by ICP-MS—Purified DMAV (8 ml, 10 μmol/liter, in PBS) was initially incubated with EDTA (20 mmol/liter) for 30 min and dialyzed against 2 liters of PBS, pH 7.4 (eight changes over 4 days). Then 1 ml of DMAV (10 μmol/liter) was incubated sep-

arately with 30 μmol/liter each of Cu^{2+}, Mn^{2+}, Ni^{2+}, Co^{2+}, and Zn^{2+} for 40 min, followed by extensive dialysis against 2 liters of Hepes (2 mmol/liter), pH 7.4 (eight changes over 3 days). In the displacement assays, DMAV (10 μM) was incubated first with a mixture containing 15 μmol/liter each of Mn^{2+}, Ni^{2+}, Co^{2+}, and Zn^{2+} for 40 min, followed by the addition of 15 μmol/liter Cu^{2+} and dialysis as above. In the competition assays, DMAV (10 μmol/liter) was incubated with a mixture of 15 μmol/liter each of Mn^{2+}, Ni^{2+}, Co^{2+}, Zn^{2+}, and Cu^{2+} for 40 min and dialyzed against 5 mM Hepes, pH 7.4. One ml of each ion-DMAV complex was used for ICP-MS.

Fluorescence Spectroscopy—Spectroscopy was carried out in a Jasco J-815 fluorospectrophotometer. Tryptophan fluorescence emissions were collected following excitation at 278 nm at a DMAV concentration of 20 μmol/liter in 1 ml of TBS, pH 7.4, using quartz cuvettes (1-cm light path). Solutions of 2 mmol/liter of $CuSO_4$, $ZnSO_4$, or Li_2SO_4 were prepared in TBS, pH 7.4. Each salt was added in 1-μl increment aliquots, followed by emission scanning between 300 and 420 nm, with a maximum at 346 nm. Scanning was performed three times for each concentration, and the results were reported as the average for three runs. To calculate the apparent kDa, data points representing the fluorescence quenching values were fitted using non-linear regression using a single-site hyperbola model.

Isothermal Titration Calorimetry (ITC)—Prostanoids (in ethanol or methyl acetate) were placed in glass vials, and the vehicle was evaporated under a nitrogen atmosphere; the dried material was then resuspended in appropriate concentrations in 20 mmol/liter Tris-HCl, 0.15 mol/liter NaCl, pH 7.4, sonicated, and vortexed as described (30). Calorimetric assays for measuring DMAV binding to a number of ligands were performed using a VP-ITC microcalorimeter (Microcal, Northampton, MA) at 30 °C. Titration experiments were performed by making successive injections of 10 μl each of 40 μmol/liter ligand into the 1.34-ml sample cell containing 4 μmol/liter DMAV until near saturation was achieved. Prior to the run, the proteins were dialyzed against 20 mmol/liter Tris-HCl, 0.15 mol/liter NaCl, pH 7.4, for binding experiments. The calorimetric enthalpy (ΔH_{cal}) for each injection was calculated after correction for the heat of the DMAV dilution obtained in control experiments performed by titrating DMAV into buffer. The binding isotherms were fitted according to a model for a single set of identical binding sites by nonlinear squares analysis using Microcal Origin software (OriginLab, Northampton, MA).

Surface Plasmon Resonance (SPR)—All SPR experiments were carried out in a T100 instrument (Biacore Inc., Uppsala, Sweden) following the manufacturer's instructions. For immobilization using an amine-coupling kit (Biacore), CM5 chips were activated with 1-ethyl-3-(dimethylaminopropyl) carbodiimide and *N*-hydroxysuccinimide before injection of DMAV (10 μg/ml) in acetate buffer, pH 5.0. Remaining activated groups were blocked with 1 mol/liter ethanolamine, pH 8.5, resulting in a final immobilization of 593.7 RU. Kinetic experiments were carried out by injecting different glycans, 500,000-Da dextran sulfate (DS500K), 50,000-Da dextran sulfate (DS50K), heparin (20 kDa), and heparin sulfate (14 kDa), for a contact time of 120 s at a flow rate of 30 μl/min at 25 °C. For all runs, HBS-P buffer was used (10 mmol/liter HEPES, 150 mmol/liter NaCl, 0.005% surfactant P20, pH 7.4). DMAV-sulfated glycan complex dissociation was monitored for 600 s, and the sensor surface was regenerated by a pulse of 30 s of 1 mol/liter NaCl at 30 μl/min. For all experiments, blank flow cells were used to subtract the buffer effect on sensorgrams. After subtraction of the contribution of bulk refractive index and nonspecific interactions with the CM5 chip surface, the individual association (k_a) and dissociation (k_d) rate constants were obtained by global fitting of data using interaction models (bivalent ligand or two-state reaction) using BIAevaluation™ (BIAcore AB, Uppsala, Sweden). Values were then used to calculate the equilibrium constant (K_D). Conditions were chosen so that the contribution of mass transport to the observed values of K_D was negligible. In addition, models in the T100 evaluation software fit for mass transfer coefficient to mathematically extrapolate the true k_a and k_d. For some analytes (DS50 and DS500), the dissociation was too slow to calculate the dissociation rate constant, and the K_D was calculated using affinity (steady-state) mode, which indicates concentration dependence binding at equilibrium levels. For some experiments, several sulfated glycans (diluted in HBS-P) were injected for 90 s with a dissociation time of 300 s. In some experiments, DMAV was used to interact with biotinylated heparin, immobilized as follows. Neutravidin (40 μg/ml; Pierce) in acetate buffer, pH 5.0, was immobilized in a CM5 chip for 7 min (10 μl/min), resulting in 2,000 RU, and blocked with ethanolamine. Then, biotinylated heparin (10 μg/ml in HBS-P; Sigma-Aldrich) was applied to the chip at a flow rate of 20 μl/min until it reached ~100 RU. DMAV was injected at a flow rate of 10 μl/min, with an association time of 30 s and dissociation time of 300 s. The chip was regenerated by a 30-s pulse with 1 mol/liter NaCl.

Interaction of DMAV with Heparin-Agarose—A HiTrap-heparin-HP column (5 ml; GE Healthcare) was connected to an AKTA purifier system (Amersham Biosciences). Before use, the column was extensively washed with 2 mol/liter NaCl. The column was then equilibrated with 10 mmol/liter Tris, 0.15 mol/liter NaCl (TBS) at a flow rate of 1 ml/min. DMAV (200 μl at 12.5 μmol/liter in TBS) was loaded into the column, followed by washing for 20 min with TBS. No increase in absorbance was observed in the flow-through. Then a 0–2 mol/liter NaCl gradient (in TBS) at 1 ml/min was performed for 40 min.

Interaction of DMAV with Phospholipid Vesicles and Platelet Membranes—DMAV (3 μmol/liter) was incubated with PC/PS (10 μmol/liter) in 10 mmol/liter TBS (pH 7.4) supplemented with $CaCl_2$ (5 mM). After 30 min, the mixture was centrifuged to separate pellet and supernatant. NuPAGE sample buffer containing 5% β-mercaptoethanol was added to the samples and loaded in a 4–12% NuPAGE gel. Gels were Coomassie Blue-stained. DMAV that had not been incubated with PC/PS was used as a control. In other experiments, washed platelets (resuspended in Tyrode's buffer without BSA or gelatin) were incubated with PBS (control) or Horm collagen (10 μg/ml) for 4 min under agitation in a Lumi-Aggregometer in the presence or absence of DMAV. Pellet and supernatant were obtained as above. DMAV that had not been incubated with platelets was used as control.

Other Assays—Recalcification time, endothelial cell proliferation, vasodilation activity, and complement inhibition assays were performed exactly as described in detail previously (4, 30, 36).

Statistical Analysis—Results are expressed as mean ± S.E. (GraphPad Software, Inc., San Diego, CA). Statistical significance was set at $p < 0.05$ (t test or analysis of variance). For ICP-MS experiments, absolute expanded uncertainty for the results is 50% of the measured value, whereas the relative expanded uncertainty is 20% of the measured value for results of the same batch/measurement.

RESULTS

Antigen-5 Family of Salivary Proteins and Phylogenetic, Biochemical, and Biophysical Properties—Fig. 1*A* shows the alignment of antigen-5 family members from several bloodsucking arthropods. Most proteins are 20–25 kDa with distinct pI values containing four cysteines and four histidines, which are highly conserved at positions His^{52}, His^{100}, His^{160}, and His^{215} (numbering system based on the sequence of DMAV). Other highly conserved clusters of amino acids are VGC and LVCNY. DMAV also exhibits a cluster of basic lysine residues in the C terminus, which may contribute to protein interaction with negatively charge molecules. Antigen-5 members belong to an expanded family of proteins from several blood-sucking arthropods whose phylogenetic associations are present in Fig. 1*B*.

To determine the function of the antigen-5 family of proteins, one member from *D. maxima* SGs was cloned, expressed, and refolded in a buffer containing 1 mmol/liter EDTA, 300 mmol/liter arginine, and oxidized and reduced glutathione at pH 9.3. The recombinant protein was purified through four chromatography steps, including two runs in gel filtration columns, one in an anion exchange column (Mono Q), and one in a cation exchange column (not shown). The purity of this preparation was assessed by one additional step in a reversed-phase column where only one peak was observed (not shown) and SDS-PAGE, which reveals one single band under denaturing or reducing conditions (Fig. 1*C*, *inset*). The N terminus of DMAV (MQ*X*QNSNQFLGSLEITGKYR) was determined by Edman degradation and is identical to the sequence predicted by the cDNA for the mature protein. The mass of the recombinant protein (25,337 Da) was also confirmed by tandem MS (Fig. 1*C*) and is compatible with the molecular mass as predicted by the cDNA (25,341 Da), with an additional methionine used for expression purposes.

Next, DMAV was examined by analytical SEC-MALS-QELS-HPLC to determine solution state, molar mass, and hydrodynamic radius. Analysis of DMAV by SEC-HPLC indicated that 100% of the protein was monomeric in solution with a retention time of 19.018 min (Fig. 1*D*). Further analysis of DMAV by in-line MALS indicated that the weight average molar mass, 28.8 kDa, of the monomeric peaks is similar to the theoretical mass of 25,341 kDa (Fig. 1*D*), suggesting a globular shape of the protein. To further characterize the tertiary structure of DMAV, the hydrodynamic radius (R_h) of the monomeric recombinant protein was examined by QELS. The R_h of DMAV was 2.8 nm, indicating that the monomeric form of the protein is globular-like. Next, CD spectra of DMAV were generated to examine its secondary structures, which were characterized by an increased intensity in negative ellipticity between 205 and 235 nm or decrease from 190 to 205 nm (Fig. 1*E*). Fig. 1*E* (*inset*) shows the percentage distribution of secondary structures in DMAV: α-helices (22.6 ± 4.8%), β-sheet (30.0 ± 4.4%), β-turn (16.1 ± 4.2%), and random (30.7 ± 4.8%).

DMAV was tested in a number of screening assays in an attempt to discover its function. DMAV (1 μmol/liter) did not prolong the recalcification time or interfere with endothelial cell proliferation. It did not produce vasodilation or inhibit the complement cascade (data not shown).

DMAV Specifically Inhibits Collagen-induced Platelet Aggregation—When tested in platelets, DMAV was found to inhibit collagen-induced platelet aggregation. The specificity of DMAV as a platelet aggregation inhibitor was then verified. Fig. 2*A* shows that only low doses (<1 μg/ml) of collagen-induced platelet aggregation are inhibited dose-dependently by DMAV. No effects on shape change were observed, suggesting that the inhibitor does not interfere with a proximal pathway of platelet activation (*i.e.* collagen-receptor interaction). It has also been noticed that platelets from some donors were more sensible to inhibition by DMAV than others. In addition, our results demonstrate that DMAV does not affect platelet aggregation by moderate to high doses of collagen or any concentration tested for a number of agonists, including convulxin, thrombin, arachidonic acid, TXA_2/PGG_2 mimetic U46619, native PGG_2, PGH_2, ADP, and PAF.

Because DMAV appears to be a specific inhibitor of collagen-induced platelet aggregation, we verified whether it blocks platelet-collagen interactions. Fig. 2*B* demonstrates that DMAV does not affect platelet adhesion to collagen (positive controls with EDTA). Surface plasmon resonance experiments also shows that DMAV does not interact with recombinant GPVI (positive control with convulxin) (Fig. 2*C*). Low doses of collagen-mediated platelet aggregation are particularly dependent on secondary mediators ADP and TXA_2 or native PGG_2/PGH_2 (37). Whereas DMAV fails to block aggregation by these agonists, we also confirmed by ITC that DMAV does not bind to either ADP or $cTXA_2$ (Fig. 2*D*). 12-H(P)ETE, a derivative of the 12-lipoxygenase that reportedly participates in platelet aggregation by collagen, also consistently failed to bind to DMAV. In addition, 26 other ligands, including U46619, TXB_2, U51605, PGH_2, $PGF_{2\alpha,\ PGD2}$, PGJ_2, PGE_2, PGE_1, 8-iso-$PGF_{2\alpha}$, iloprost, 5(*S*)-HETE, 15(*S*)-HETE, 20-HETE, L-oleoyl-lysophosphatitic acid, sphingosine 1-phosphate, arachidonic acid, PAF, LTB_4, LTC_4, LTD_4, LTE_4, epinephrine, norepinephrine, histamine, and serotonin, tested negative for binding to DMAV (not shown). Together, these experiments suggested that DMAV affects platelets by a mechanism that is clearly distinct from other salivary inhibitors of collagen-induced platelet aggregation (2).

Antigen-5 Member from T. infestans Salivary Gland Also Inhibits Platelet Aggregation—Besides DMAV, a second member of the antigen-5 family was expressed from *T. infestans* (TIAV) in order to verify whether the anti-platelet function was conserved. Fig. 3*A* compares the SDS-PAGE for both DMAV and TIAV, which exhibits the expected molar masses. Fig. 3*B* demonstrates that TIAV inhibits platelet aggregation by low

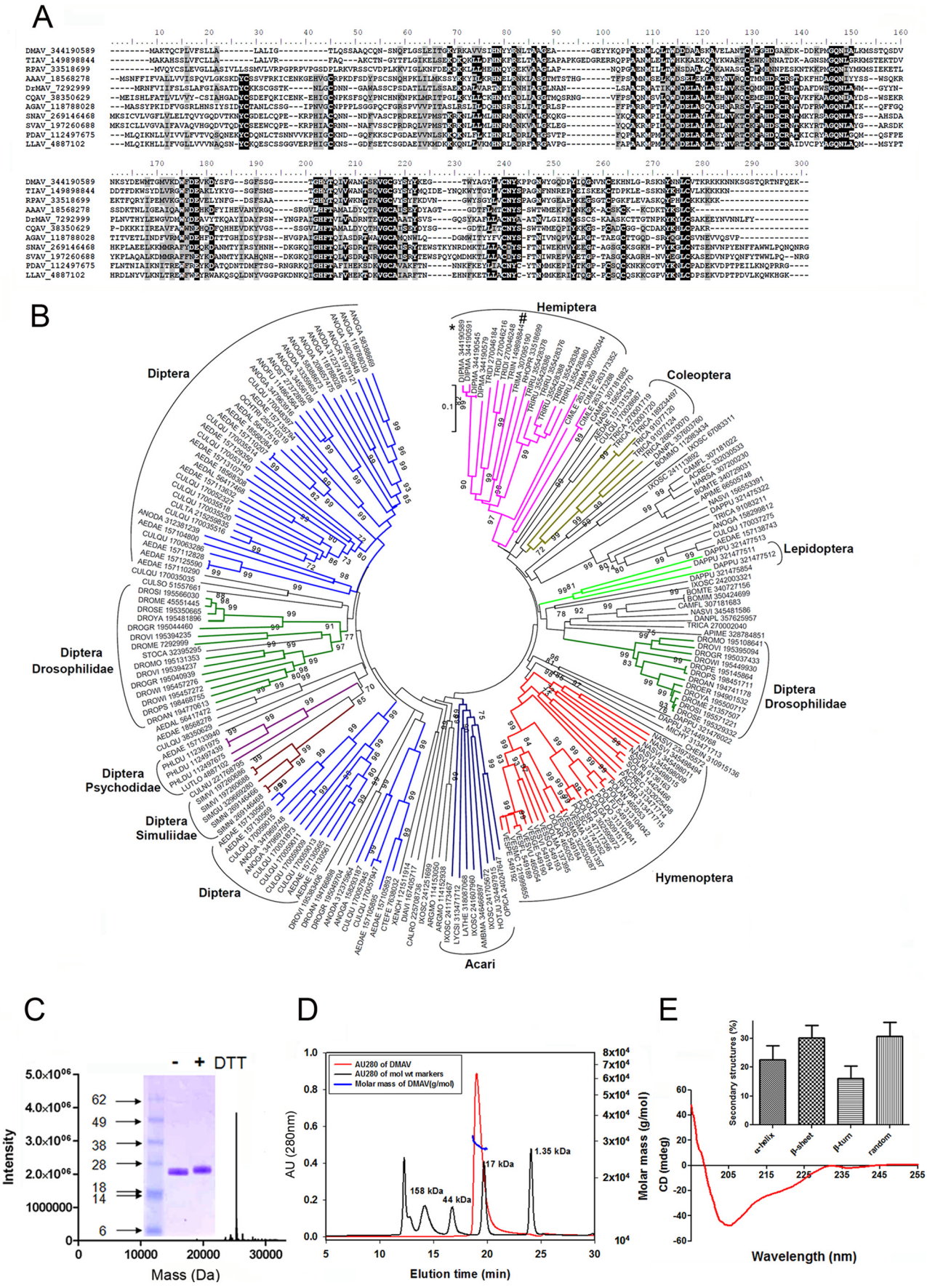
A
B
Hemiptera
Coleoptera
Lepidoptera
Diptera
Drosophilidae
Diptera
Drosophilidae
Diptera
Psychodidae
Diptera
Simuliidae
Diptera
Hymenoptera
Acari
C
- + DTT
Intensity
Mass (Da)
D
AU280 of DMAV
AU280 of mol wt markers
Molar mass of DMAV(g/mol)
AU (280nm)
Molar mass (g/mol)
Elution time (min)
158 kDa
44 kDa
17 kDa
1.35 kDa
E
Secondary structures (%)
α-helix
β-sheet
β-turn
random
CD (mdeg)
Wavelength (nm)

doses of collagen (0.5 μg/ml). Because collagen, but not ADP or thrombin, is the only platelet agonist that consistently promotes an increase of extracellular $O_2^{\cdot-}$ (10, 11), it was hypothesized that antigen-5 members might affect the pro-aggregatory properties of ROS on platelets. Therefore, we compared the effects of TIAV with Cu,Zn-SOD. Fig. 3*B* also shows that Cu,Zn-SOD, like TIAV, attenuates platelet aggregation (but not the shape change) by collagen (0.5 μg/ml). On the other hand, arachidonic acid (58 μmol/liter)-induced aggregation is not affected by both inhibitors (Fig. 3*C*). We also tested the effects of TIAV in other parameters of platelet activation. Fig. 3, *D* and *E*, demonstrate that TIAV dose-dependently inhibits platelet ATP secretion and TXA_2 generation induced by collagen, respectively. Because it has been reported that NADPH oxidase inhibitors, such as diphenylene iodonium and apocynin, partially attenuate thrombus formation triggered by a collagen surface at high shear rates *in vitro* (38), we tested TIAV in this assay. Fig. 3*F* (*left panel*) shows thrombus formation in control experiments. In the presence of TIAV (3 μmol/liter; Fig. 3*F*, *right panel*), a slight effect could be observed in the shape of the thrombus; however, this effect was variable and dependent on the donor, being difficult to consistently quantify.

DMAV Scavenges $O_2^{\cdot-}$—Experiments with platelets supported the hypothesis that DMAV operates through scavenging of $O_2^{\cdot-}$. To test this, we employed PMA-stimulated neutrophils, which generate intense production of $O_2^{\cdot-}$ through activation of NADPH oxidases. Our results show that DMAV dose-dependently inhibits the signal due to $O_2^{\cdot-}$ when evaluated by either Diogenes reagent (Fig. 4*A*) or lucigenin (Fig. 4*B*) with IC_{50} of ~0.5 μmol/liter. We also tested the effects of DMAV in $O_2^{\cdot-}$ generated in a cell-free system by X/XO according to Reaction 1.

$$\text{Hypoxanthine} + O_2 + H_2O \xrightarrow{\text{XO}} \text{Uric acid} + O_2^{\cdot-} + H^+$$

REACTION 1

Fig. 4*C* demonstrates that DMAV diminishes the $O_2^{\cdot-}$ signal (detected by Luminol) with concentrations similar to those observed with neutrophils. In contrast, a number of other available recombinant salivary proteins expressed in *E. coli* (*e.g.* DM146, triplatin, SVEP, yellow protein) or in insect cells (*e.g.* ixolaris, 9.3 kDa) and purified as described for DMAV were ineffective in the same assay (Fig. 4*D*).

To confirm the antioxidant activity of DMAV using another detection method, we evaluated its effects in the cyt *c* reduction assay using X/XO to generate $O_2^{\cdot-}$ *in vitro*.

Fig. 4*E* demonstrates that DMAV produces partial inhibition of cyt *c* reduction, whereas three other recombinant proteins (ixolaris, dipetalodipin, and BSA) were without effect. We also determined that the enzymatic activity of X/XO, evaluated by production of uric acid, was unaffected by DMAV (Fig. 4*F*). Altogether, it was hypothesized that DMAV operates either as a non-catalytic scavenger of $O_2^{\cdot-}$ (33) or as an enzyme (*e.g.* Cu,Zn-SOD) that could dismutate $O_2^{\cdot-}$ to H_2O_2 (39), according to Reactions 2 and 3, where M is metal.

$$M^{(n+1)+}\text{-SOD} + O_2^{\cdot-} \rightarrow M^{n+}\text{-SOD} + O_2$$

$$M^{n+}\text{-SOD} + O_2^{\cdot-} + 2H^+ \rightarrow M^{(n+1)+}\text{-SOD} + H_2O_2$$

REACTIONS 2 and 3

To test whether DMAV also generates H_2O_2, peroxide production was estimated using Amplex Red reagent in reactions started with X/XO. In contrast to Cu,Zn-SOD, which increases H_2O_2 formation, DMAV did not increase its production (Fig. 4*G*).

DMAV was also tested to determine whether it works as a catalase according to Reaction 4.

$$2\ H_2O_2 \rightarrow 2\ H_2O + O_2$$

REACTION 4

An H_2O_2 standard curve was constructed, followed by incubation for 15 min with PBS or DMAV. H_2O_2 was detected with Amplex Red. Fig. 4*H* shows that no change in the concentration of H_2O_2 was observed. We aimed to determine whether DMAV displays catalase activity using a direct method using a Clark electrode, which measures oxygen concentration in a solution (33). In this experiment, the solution containing xanthine exhibited an oxygen concentration of ~280 μM. When XO was added to the chamber (under stirring conditions), the generation of $O_2^{\cdot-}$ was accompanied by consumption of O_2, detectable by a continuous downward inflection of the pen (Fig. 4*I*). After 15 min, most O_2 that has been converted to $O_2^{\cdot-}$ will spontaneously dismutate to stable H_2O_2. Accumulation of H_2O_2 can be detected by the addition of catalase (control) to this solution, because conversion of H_2O_2 into O_2 and water produces an increase in O_2 levels according to Reaction 4, which is detected by a sharp upward inflection of the pen (Fig. 4*I*). When the experiments were performed as above but DMAV was added instead of PBS, no change in oxygen consumption was noticed. Furthermore, after the addition of catalase, the same change in $O_2^{\cdot-}$ formation was observed (relative to PBS), implying that DMAV is devoid of catalase activity.

FIGURE 1. **Characterization of DMAV.** *A*, Clustal alignment of DMAV (gi 344190589) and antigen-5 members from *T. infestans* (TIAV; gi149898844), *Rhodnius prolixus* (RPAV; gi33518699), *Aedes aegypti* (AAAV; gi 18568278), *Drosophila melanogaster* (DrMAV; gi 7292999); *Culex quinquefasciatus* (CQAV; gi38350629); *Anopheles gambiae* (AGAV; i118788028); *Simulium nigrimanus* (SNAV; gi 269146468); *Simulium vitatum* (SVAV; gi 197260688), *Phlebotomus duboscqi* (PDAV; gi112497675), and *Lutzomyia longipalpis* (LLAV; gi4887102). *B*, phylogenetic tree for antigen-5 family members from several blood sucking salivary glands. Two antigen-5 members studied herein are indicated as DMAV (*) or TIAV (#). *C*, purity of DMAV. An aliquot of purified DMAV was used for mass spectrometry and yielded a mass of 25,337 Da (predicted mass, 25,341 Da). *Inset* on the *left*, SDS-PAGE of DMAV. Three μg of DMAV under non-reducing (*DTT*−) or reducing (*DTT*+) conditions was applied to 4–12% NuPAGE. Molecular weight markers are show on the *left*. *D*, biophysical properties of DMAV. Analysis by SEC-MALS-HPLC provided the molar mass distribution of the main peak compared with absorbance at 280 nm. Molecular weight markers were loaded in the same column, and elution volume was compared with DMAV (*arrow*, *inset*) (inline multiangle light scatter). The *solid* and *red lines* represent absorbance 280 nm and MALS results, respectively. *E*, CD analysis of DMAV in aqueous solution. The ellipticity (degrees cm^2/dmol) was plotted as a function of wavelength (nm). *Inset*, percentage of secondary structures.

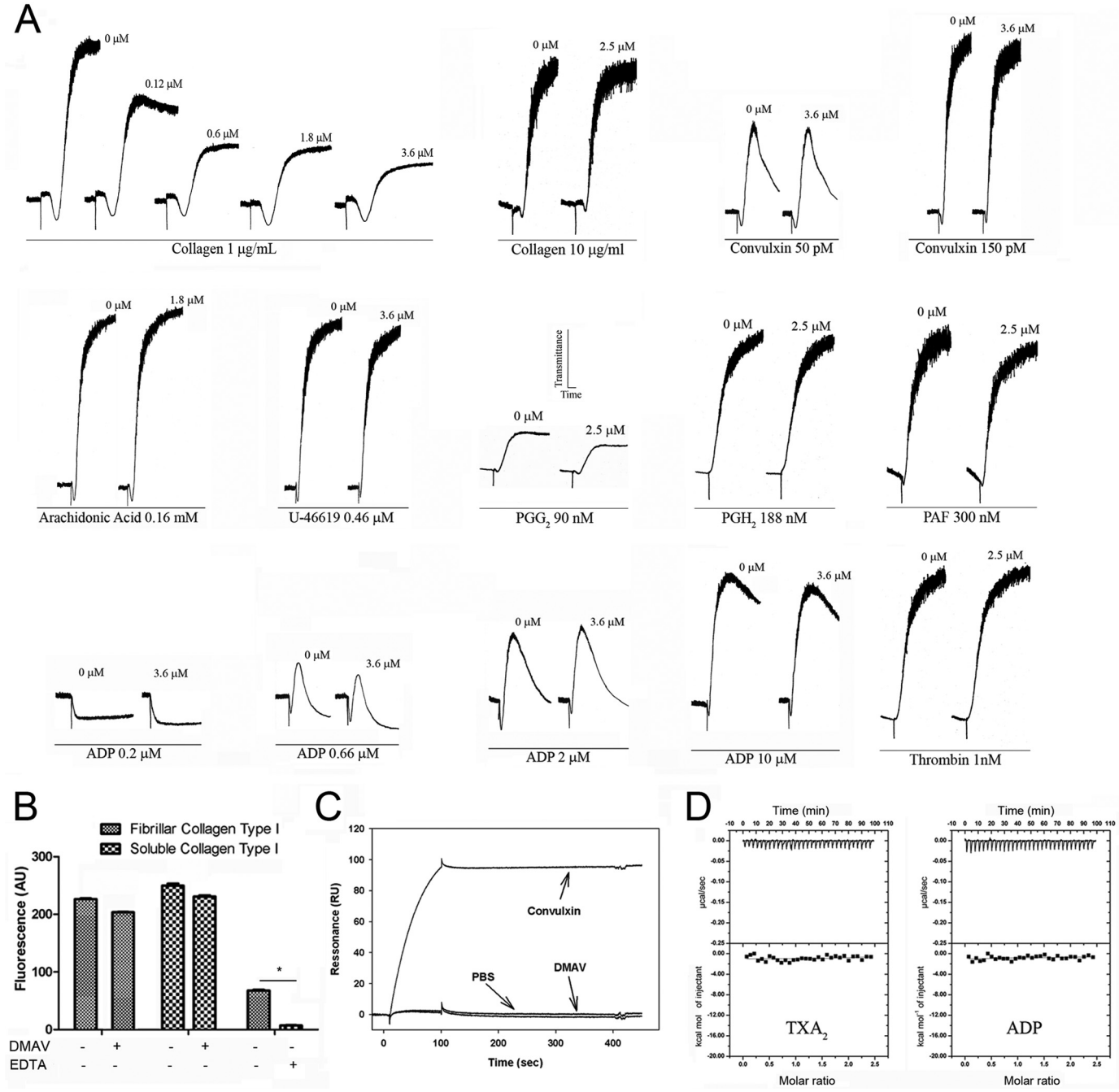

FIGURE 2. **DMAV inhibits collagen-induced platelet aggregation.** *A*, human platelet-rich plasma ($2 \times 10^5/\mu$l) was incubated with DMAV for 1 min (concentrations are given for each trace) followed by the addition of different platelet agonists, as indicated. Platelet aggregation was estimated by turbidimetry under test tube-stirring conditions. Washed human platelets were employed when thrombin was used as an agonist. The traces represent a typical experiment. *B*, DMAV does not affect platelet adhesion to fibrillar or soluble collagen I immobilized in 96-well plates. Calcein-AM-labeled platelets were added to the wells and incubated for 1 h at 37 °C. Wells were washed with Tyrode-BSA. EDTA was used as a control. Fluorescence was detected with excitation at 485 nm and emission at 530 nm. Significance (*) was set at $p < 0.05$ (*t* test). *C*, DMAV does not interact with GPVI by SPR. GPVI was immobilized in a CM5 sensor chip, and DMAV was used as an analyte. No increase in resonance was observed in the presence of DMAV (1 μM). Convulxin (10 nmol/liter), a GPVI ligand, was used as positive control. *D*, isothermal titration calorimetry for ADP or $cTXA_2$ interaction with DMAV. *Top panels*, base line-adjusted heats per injection of ADP (20 μmol/liter) or cTXA2 (20 μmol/liter) into DMAV (2.0 μmol/liter). *Bottom panels*, molar enthalpies per injection for ADP or $cTXA_2$ interaction with DMAV. No binding was observed.

Proteins exhibit antioxidant activity through three distinct mechanisms (*i.e.* methionine oxidation (40), cysteine oxidation (41), and metal oxidation (39)). To verify whether free cysteines with the potential to scavenge O_2^- are present in DMAV, the protein was incubated with benzofurazone 4-fluoro-7-aminosulfonylbenzofurazan, which reacts with free cysteines. No increase over basal levels of the fluorescence of DMAV was observed. As a control, free cysteines or reduced DMAV produced a strong fluorescence signal (not shown). It is concluded that DMAV does not contain free cysteines that could mediate its antioxidant activity. To verify whether methionines in DMAV were oxidized, the protein was incubated with X/XO, and its mass was evaluated by MS. No change in mass compatible with methionine oxidation was observed (not shown).

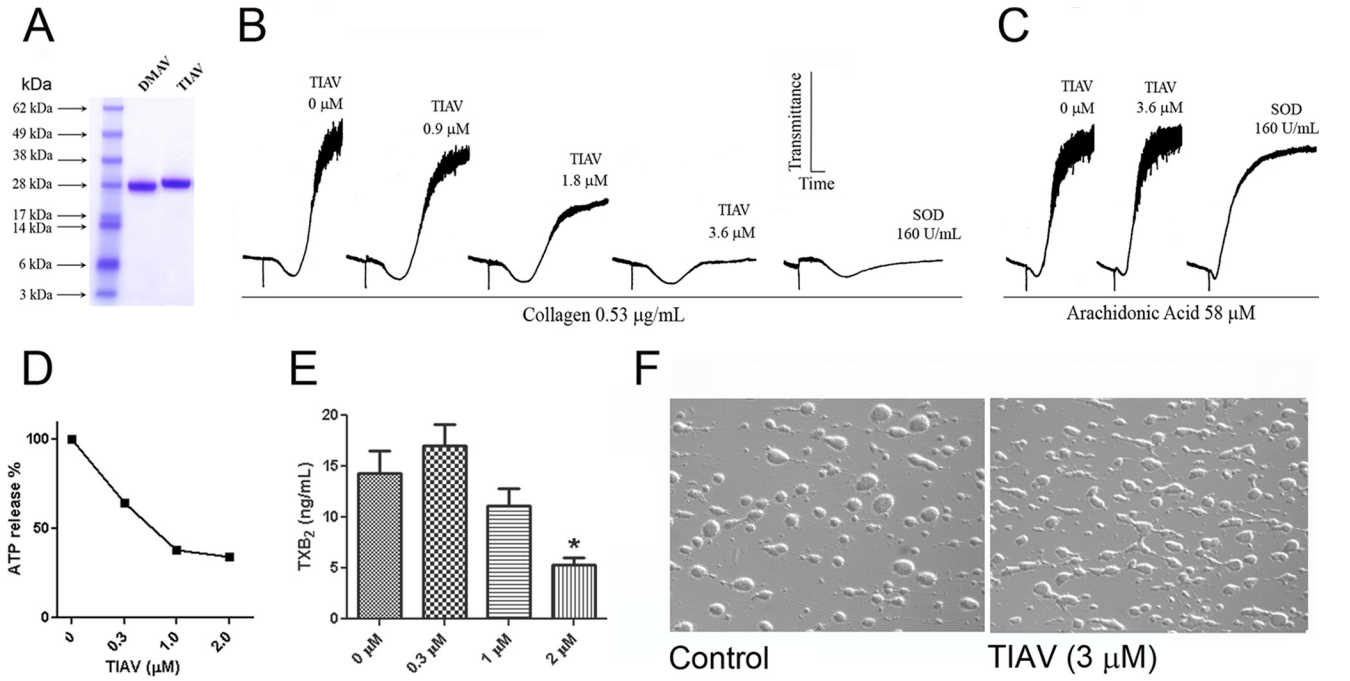

FIGURE 3. **TIAV, another family member, inhibits collagen-induced platelet aggregation.** *A*, SDS-PAGE for recombinant purified DMAV and TIAV. *B*, TIAV inhibits collagen-induced platelet aggregation which is comparable with Cu,Zn-SOD. *C*, neither TIAV nor Cu,Zn-SOD (160 units/ml) inhibit arachidonic acid-induced platelet aggregation. *D*, TIAV inhibits collagen-induced ATP secretion (estimated by luciferin-luciferase); *E*, TXB_2 production was detected by ELISA. Significance (*) was set at $p < 0.05$. *F*, TIAV only marginally attenuated thrombus formation in a collagen surface at high shear rates. Experiments were performed with different donors ($n = 3$). *Error bars*, S.E.

Next, DMAV was incubated with EDTA to chelate metals potentially bound to the protein. Fig. 4*J* shows that DMAV loses its antioxidant activity in the presence of EDTA (5 mmol/liter), which is consistent with a metal-dependent activity. In contrast, no inhibition of the antioxidant activity of Cu,Zn-SOD was detected, because it tightly interacts with Cu^{2+}/Zn^{2+} (42). The distinct sensitivity of DMAV and Cu,Zn-SOD for EDTA also implies that our preparation is devoid of contaminating *E. coli* Cu,Zn-SOD.

DMAV Binds Divalent Metal and ICP-MS Results—To estimate the metal content of recombinant DMAV, a highly purified sample was applied to ICP-MS, which is the most sensitive method available to evaluate metals and other ions present in a given sample (35). Fig. 5*A* presents the ratio (ion content in the sample, ng/g)/(ion content in the buffer, ng/g) in the preparation. The results indicate that DMAV binds Co^{2+}, Zn^{2+}, and Cu^{2+}. In addition, Ni^{2+} was found in our sample (not shown), which is often a contaminant detected by ICP-MS. No other ion of the periodic table was found to interact with DMAV. Next, we evaluated whether DMAV binds additional metals provided in purified form. For these experiments, DMAV was incubated with EDTA and extensively dialyzed against Hepes-saline. Each metal (30 μmol/liter) was added to DMAV (10 μmol/liter), and after 30 min, the mixture was again extensively dialyzed. Fig. 5*B* demonstrates that DMAV equally binds Cu^{2+}, Mn^{2+}, Ni^{2+}, Co^{2+}, and Zn^{2+}. When no metal was added to DMAV, only trace amounts of Zn^{2+} and Cu^{2+} were identified in the sample, indicating DMAV bound to trace metals present in the buffer. Next, the relative specificity of DMAV for Cu^{2+} and other metals was evaluated. In competition assays, DMAV was added to a mixture containing equal concentrations of Cu^{2+}, Mn^{2+}, Ni^{2+}, Co^{2+}, and Zn^{2+} followed by dialysis. Only Cu^{2+} was identified in the preparation (Fig. 5*C*). In displacement assays, DMAV was incubated with Mn^{2+}, Ni^{2+}, Co^{2+}, and Zn^{2+}, followed by the addition of Cu^{2+}, and dialyzed. Fig. 5*D* demonstrates that only Cu^{2+} was found associated with DMAV.

Fluorescence Spectroscopy for DMAV—Tryptophan fluorescence spectra of metal-free and Cu^{2+}-complexed preparations of DMAV were employed to determine the relative affinity of the interaction identified by ICP-MS. The addition of $CuSO_4$ induced quenching of the fluorescence to 30% of the initial intensity, suggesting that tryptophan indoles moved to a more hydrophobic environment (Fig. 6*A*). In contrast, no change in intrinsic fluorescence was observed when Li_2SO_4 was added to DMAV (Fig. 6*A*, *dotted lines*). Data points were fitted by non-linear regression to a single-site hyperbolic model, which resulted in an apparent K_D of 20.7 μmol/liter (Fig. 6*B*). This value does not reflect the true affinity of DMAV for the ion because it varies with the concentration of DMAV used in the assay (20 μmol/liter). As an additional control, no change in the intrinsic fluorescence spectroscopy was observed when $CuSO_4$ (60 μmol/liter) was added to DM146 (gi315270899), another *E. coli* expressed salivary protein from *D. maxima* (Fig. 6*C*). The UV spectrum of DMAV was performed, and peak absorbance was detected at 280 nm. Additional peaks were not observed at longer wavelengths in the presence of Cu^{+} (data not shown), in contrast to Cu^{+} oxidases (so-called "blue copper proteins") (43, 44).

Comparison of the Antioxidant Activities of Cu^{2+}-DMAV and Cu,Zn-SOD—To verify the antioxidant potential of the protein, DMAV (10 μmol/liter) previously incubated with (20 μmol/liter) Cu^{2+} was extensively dialyzed against PBS, pH 7.4.

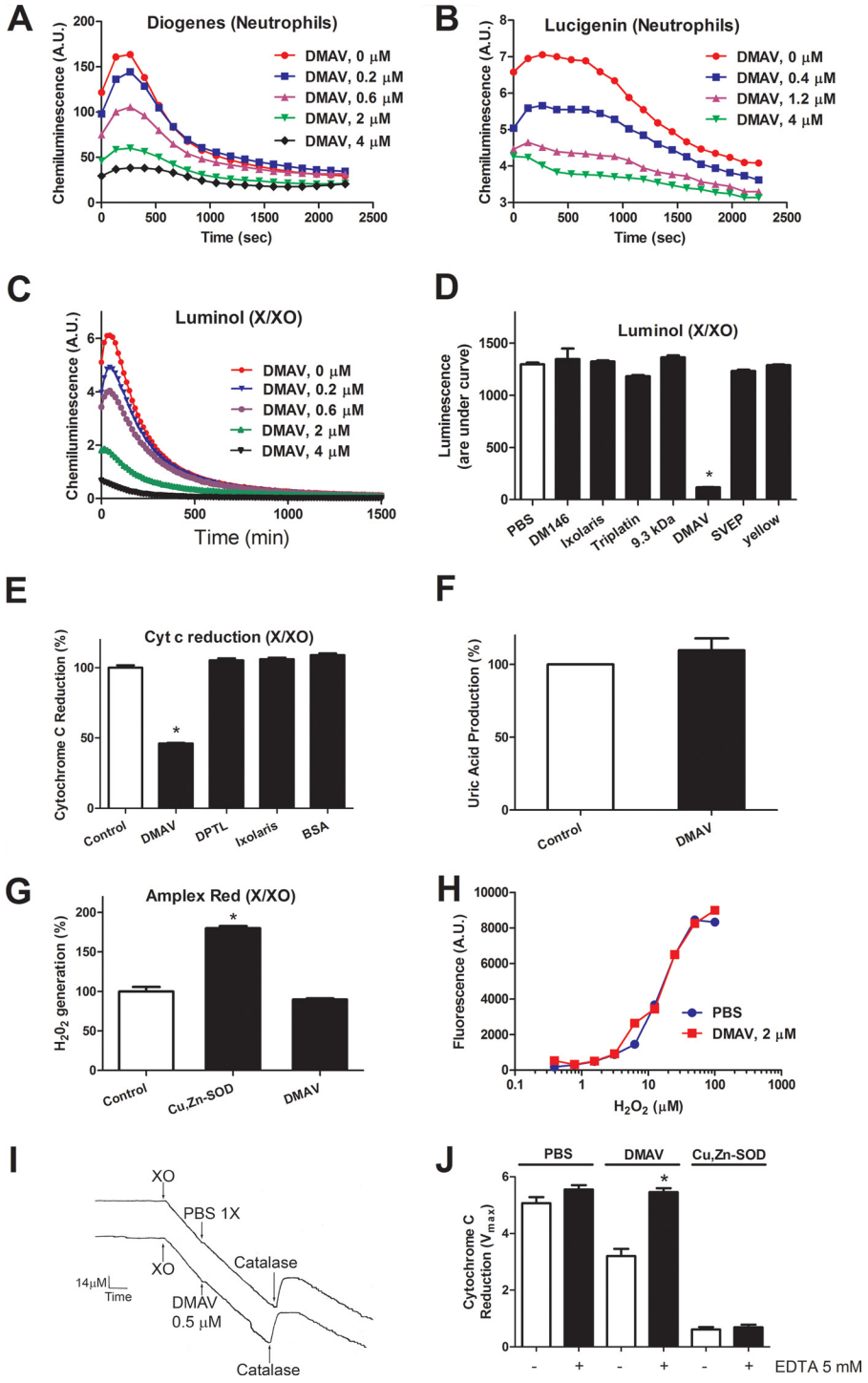

FIGURE 4. **DMAV is an antioxidant that scavenges $O_2^{\cdot-}$.** *A*, neutrophils were activated with PMA (5 nmol/liter) in the presence of increasing concentrations of DMAV. Superoxide was detected using Diogenes luminescent reagent for $O_2^{\cdot-}$. *B*, neutrophils were activated as in *A*, but $O_2^{\cdot-}$ was detected with Lucigenin (20 μmol/liter). *C*, $O_2^{\cdot-}$ was generated by an X/XO system; luminescence was detected using luminol (500 μmol/liter). *D*, several proteins (DM146, ixolaris, triplatin, 9.3 kDa, SVEP, and yellow protein; 2 μmol/liter) were expressed and purified as DMAV and tested side by side. Detection of $O_2^{\cdot-}$ was performed with Luminol (500 μmol/liter). *E*, $O_2^{\cdot-}$ was produced by the X (500 μmol/liter)/XO (1.2 milliunits/ml) system and detected by the reduction of cytochrome *c* (12 μmol/liter) at 550 nm. Other available salivary recombinant proteins (dipetalodipin (*DPTL*), ixolaris, and BSA; 2 μmol/liter) were tested side by side with DMAV (5 μmol/liter). *F*, DMAV (5 μmol/liter) does not affect the enzymatic function of X/XO, determined by uric acid production at 293 nm. *G*, effects of DMAV on generation of H_2O_2. X (500 μmol/liter)/XO (6.3 milliunits/ml) was used to generate H_2O_2, which was detected with the Amplex Red reagent. In control, spontaneous dismutation of $O_2^{\cdot-}$ is observed, which is increased in the presence of Cu,Zn-SOD (4 milliunits/ml). DMAV (5 μmol/liter) did not increase H_2O_2 production. *H*, DMAV does not display catalase activity. Different concentrations of H_2O_2 were incubated for 15 min with PBS or DMAV (2 μmol/liter) and detected with Amplex Red reagent as described under "Experimental Procedures." *I*, catalase activity. XO (0.7 milliunits/ml) was added to a solution containing hypoxanthine (500 μM), and O_2 consumption was detected with a Clark electrode. After 15 min, catalase (333 units/m) was added to the chamber, and a peak of O_2 is observed. No effects were observed after the addition of DMAV (0.5 μM). *J*, DMAV displays metal-dependent antioxidant activity. DMAV (5 μmol/liter) or Cu,Zn-SOD (0.42 unit/ml) was incubated with EDTA (5 mmol/liter) for 15 min and tested in the cytochrome *c* reduction assay. Antioxidant activity of DMAV was abolished by EDTA ($n = 3$). Significance (*) was set at $p < 0.05$ (analysis of variance). *A.U.*, arbitrary units. *Error bars*, S.E.

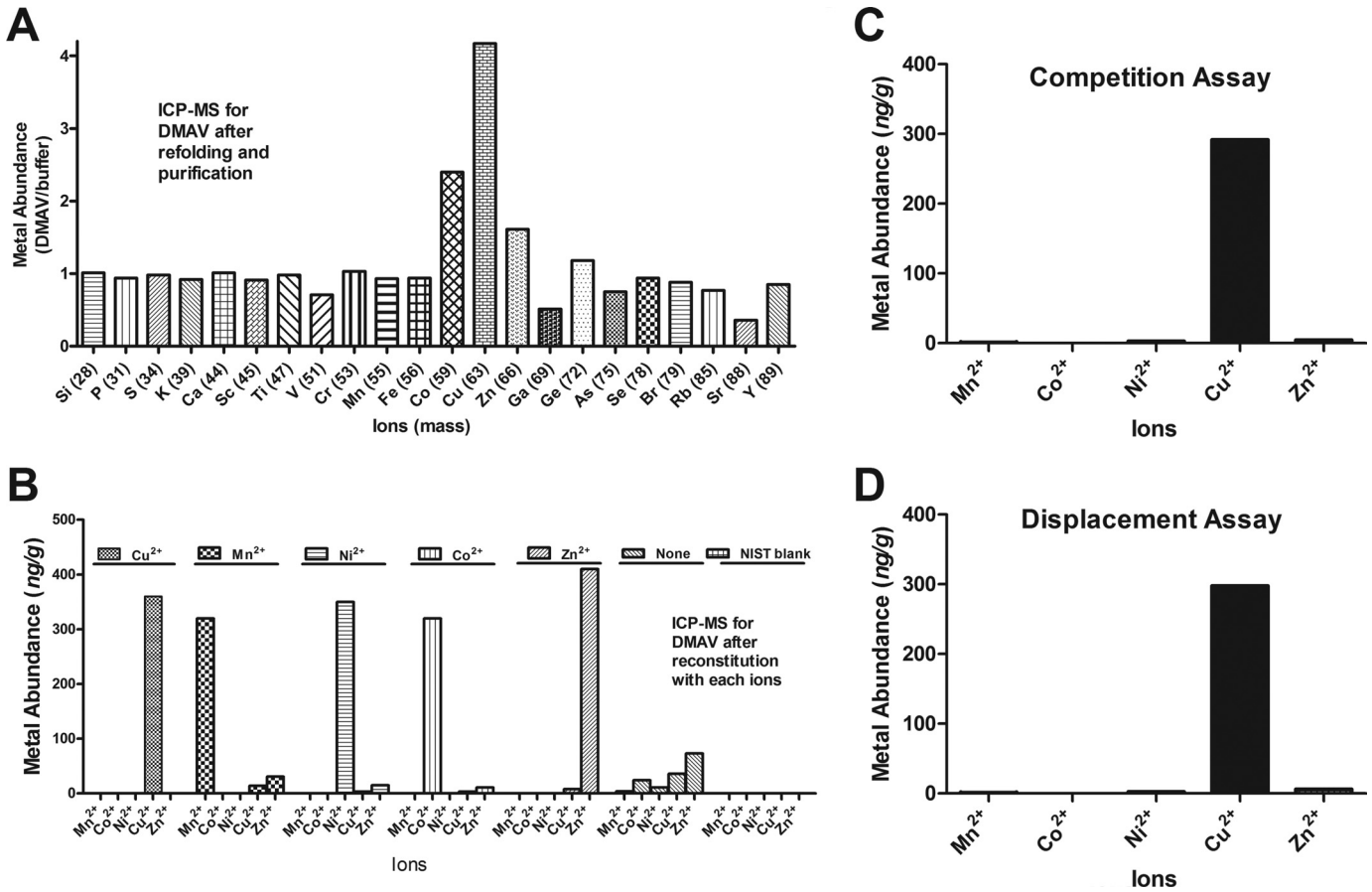

FIGURE 5. **DMAV is a Cu^{2+}-binding protein; ICP-MS results.** *A*, recombinant DMAV was used for analysis of metal content by ICP-MS. Only Cu^{2+}, Zn^{2+}, and Co^{2+} were identified. *B*, DMAV (10 μmol/liter) was incubated with EDTA followed by the addition (separately) of divalent metals (30 μmol/liter each), dialysis against Hepes (5 mmol/liter), and analysis by ICP-MS. *C*, competition assays. DMAV (10 μmol/liter) was added to a mixture containing 15 μmol/liter (each) of $MnCl_2$, $CoCl_2$, $NiCl_2$, $CuCl_2$, and $ZnCl_2$, followed by dialysis and analysis of metal content by ICP-MS. *D*, displacement assays. DMAV (10 μmol/liter) was incubated with 15 μmol/liter (each) of Mn^{2+}, Co^{2+}, Ni^{2+}, and Zn^{2+} for 30 min, followed by the addition of Cu^{2+}. After dialysis, metal content was evaluated by ICP-MS. For ICP-MS experiments (*A–D*), absolute expanded uncertainty for the results is 50% of the measured value, whereas the relative expanded uncertainty is 20% of the measured value for results of the same batch/measurement.

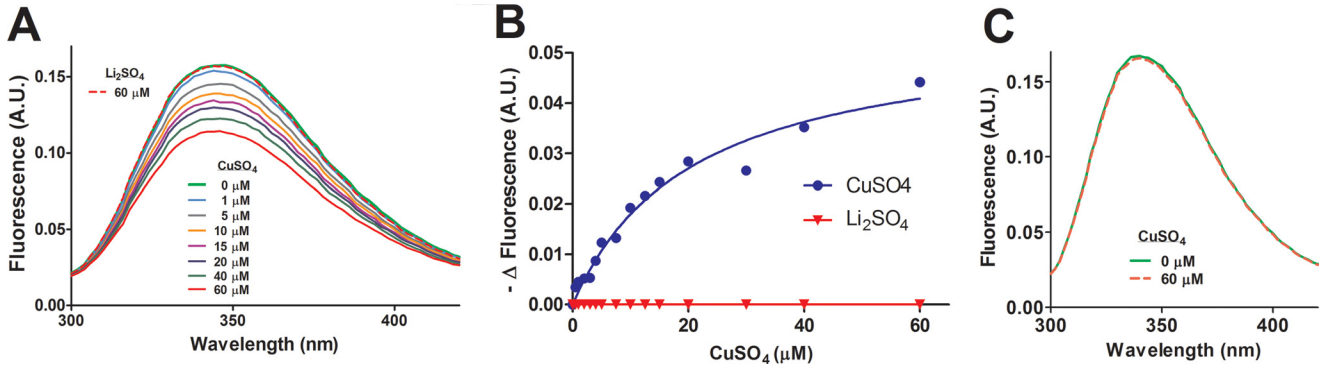

FIGURE 6. **Cu^{2+} changes the intrinsic fluorescence spectrum of DMAV.** *A*, fluorescence spectrometry. Changes of the intrinsic fluorescence of DMAV (20 μmol/liter in 1 ml of TBS, pH 7.4) was estimated with emission at 346 nm and excitation at 278 nm. $CuSO_4$ (1 mmol/liter in TBS) was added as 1-μl aliquots, resulting in final concentrations indicated in the figure. The final volume of $CuSO_4$ was 18 μl. Li_2SO_4 (18 μl at 1 mmol/liter; final concentration 60 μmol/liter) did not affect the intrinsic fluorescence of DMAV (20 μmol/liter). *B*, the change in fluorescence was used to determine apparent K_D. *C*, $CuSO_4$ (60 μmol/liter) does not change the intrinsic fluorescence of an unrelated salivary protein (DM146; 20 μmol/liter) from *D. maxima*. *A.U.*, arbitrary units.

To study the kinetics of the reaction of Cu^{2+}-DMAV with $O_2^{\cdot-}$ generated by X/XO, the rate of formation of cyt *c* reduction was spectrophotometrically monitored at pH 7.8 in the absence (*V*) and presence (v) of various Cu^{2+}-DMAV concentrations. Results obtained by this method compare well with direct measurement of $O_2^{\cdot-}$ estimated by pulse radiolysis (45). Fig. 7, *A* and *B*, show the progress curves of cyt *c* reduction with increasing concentrations of Cu^{2+}-DMAV or Cu,Zn-SOD respectively.

Fig. 7, *C* and *D*, shows the dose-response curves for the results presented in 7, *A* and *B*, respectively, with a calculated IC_{50} of ~50 nmol/liter for Cu^{2+}-DMAV and 1 nM for Cu,Zn-

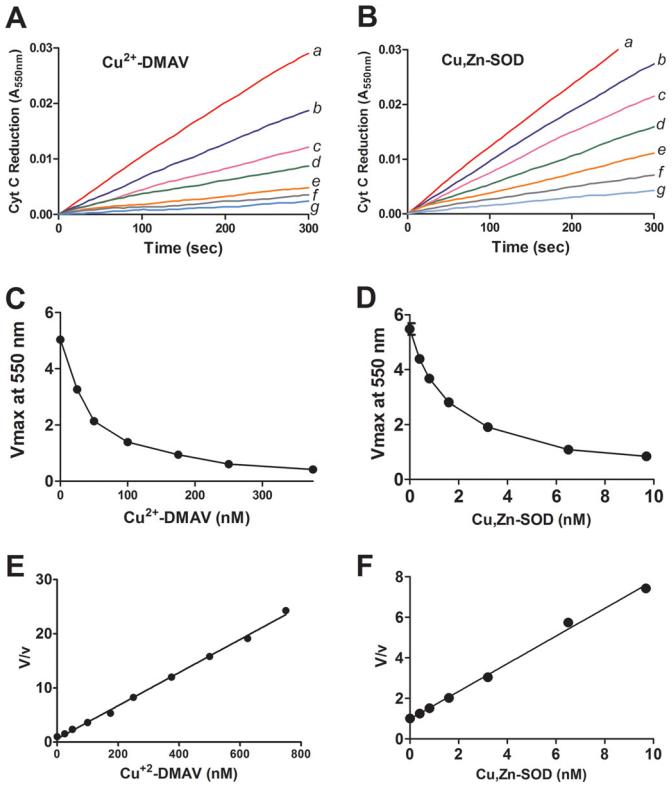

FIGURE 7. **Comparison of the antioxidant activity of Cu^{2+}-DMAV and Cu,Zn-SOD.** Cytochrome *c* reduction assays were performed by the addition of XO (1.2 units/ml) to hypoxanthine (0.5 mM) in phosphate buffer, pH 7.8, in the presence of Cu^{2+}-DMAV (*A*) (0 nM (*a*), 25 nM (*b*), 50 nM (*c*), 100 nM (*d*), 250 nM (*e*), 375 nM (*f*), or 500 nM (*g*)) or Cu,Zn-SOD (*B*) (0 nM (*a*), 0.4 nM (*b*), 0.8 nM (*c*), 1.6 nM (*d*), 3.2 nM (*e*), 6.5 nM (*f*), and 13 nM (*g*)). Progress curves are shown. Transformation of the data in *A* and *B* is shown as a function of V_{max} and [Cu^{2+}-DMAV] (nM) (*C*) or [Cu,Zn-SOD] (nM) (*D*), respectively. Transformation of the data in *C* and *D* is shown as a function of *V*/*v* and [Cu^{2+}-DMAV] (nM) (*E*) or [Cu,Zn-SOD] (nM) (*F*). *V*, initial velocity; *v*, final velocity. The linear transformation of the data suggests a catalytic process (34).

SOD. Data were analyzed by plotting *V*/*v* as a function of [Cu^{2+}-DMAV] according to Krishna *et al.* (33) (Fig. 7*E*). Fig. 7*F* shows the same transformation for Cu,Zn-SOD. From the slope of the line and knowing Kcyt-c^{III} + superoxide (33, 46) at pH 7, the k_{app} for the Cu^{2+}-DMAV interaction with O_2^- was calculated to be 0.31×10^8 mol liter^{-1} s^{-1}. This is ~30–50 times less than the K_{cat} ($2–3 \times 10^9$ mol liter^{-1} s^{-1}) observed for [Cu,Zn-SOD] (33, 39, 45–47). The antioxidant activity of Cu^{2+}-DMAV was not affected by the presence of catalase in the assay (not shown). McCord and Fridovich (48) defined the specific activity of SOD in units/mg, where 1 unit is the amount in mg of protein that inhibits 50% of the reduction of 10 μmol/liter cytochrome *c* by O_2^- (generated by the X/XO system) in a 3.0-ml reaction volume containing 50 mmol/liter phosphate buffer at pH 7.8. This is ~430 units/mg Cu^{2+}-DMAV. DMAV was devoid of antioxidant activity when preincubated with Zn^{2+} (data not shown).

DMAV Binds to Heparin and Sulfated Glycosaminoglycans—It has been reported that extracellular SOD interacts with heparin through its C terminus (49). To verify whether DMAV interacts with sulfated glycosaminoglycans, it was immobilized in a CM5 sensor chip, followed by injection of sulfated glycosaminoglycans. Fig. 8*A* shows that DS50K and DS500K avidly interact with DMAV. Binding was also detectable with heparin and heparan sulfate. In contrast, no signal was observed when non-sulfated dextran 12K, non-sulfated dextran 670K, chondroitin sulfate, or enoxaparin were used as analytes (not shown). Next, the kinetics of DMAV interaction with DS500K and DS50K were studied. Sensorgrams are shown in Fig. 8, *B* and *C*, and data were fitted with a bivalent analyte model. In both cases, the association phase was followed by a very slow dissociation rate, which does not allow precise calculation of the k_{off}. In these cases, the K_d can be determined by steady-state kinetics. Fig. 8*D* shows that DS500K and DS50K interact with immobilized DMAV in a saturable manner with a K_d of ~0.41 nmol/liter ± 0.05 nmol/liter and 1.96 nmol/liter ± 0.2 nmol/liter, respectively. Fig. 8, *E* and *F*, also demonstrates that DMAV interacts with heparan sulfate or heparin, respectively. To estimate the K_d of heparin-DMAV interactions with accuracy, biotinylated heparin was coupled to neutravidin immobilized in a CM5 chip, and DMAV was used as an analyte. Sensorgrams are depicted in Fig. 8*G*. The *inset* presents the fit of the data using steady-state kinetics, which resulted in a K_d of 97.0 ± 4.5 nmol/liter. The interaction of DMAV with heparin was also tested using a heparin-agarose column. Fig. 8*H* demonstrates that elution of DMAV was observed at ~1 mol/liter NaCl. This result provides additional evidence to conclude that DMAV is a heparin-binding protein. In order to evaluate whether DMAV binds to membranes, it was incubated with PC/PS or activated platelets as described under "Experimental Procedures." In both cases, no interaction was observed (not shown), excluding DMAV as a phospholipid-binding protein.

Antioxidant Activity Is Present in the SG of D. maxima—To examine whether the SG of *D. maxima* exhibits antioxidant activity, salivary gland homogenate (SGH) was prepared, and the supernatant was obtained after centrifugation. Fig. 9*A* shows that SGH inhibits the signal of O_2^- generated by X/XO with an IC_{50} of ~0.05 pairs/assay. In addition, SGH dose-dependently attenuated collagen (0.53 μg/ml)-induced platelet aggregation (Fig. 9*B*).

Because SGH is a complex mixture of proteins, and different molecules may exhibit antioxidant activity or inhibit platelet aggregation, our goal was to verify whether specific fraction-containing DMAV also exhibited the activities. SGH was prepared from 100 pairs of glands and supernatant loaded into a G-75 gel filtration column. Fig. 9*C* shows the elution profile of the homogenate, which was characterized by a large peak where most lipocalins (the most abundant protein family in triatomine saliva) are found. Recombinant DMAV loaded onto the same column under identical experimental conditions elutes around 11.5–12.5 min, which is compatible with its molar mass of 25 kDa (Fig. 9*D*). To determine the elution profile of native DMAV, an aliquot of each fraction was used to immobilize the protein, and an ELISA was performed using polyclonal anti-DMAV antibody as a probe. Fig. 9*E* shows that the peak of DMAV recognized by the antibodies coincides with the elution pattern of recombinant protein. To confirm the presence of DMAV in the SGH, fractions 21 and 23, which flank the maximum antibody titles indicative of DMAV by ELISA, were chosen. These fractions were loaded into a one-dimen-

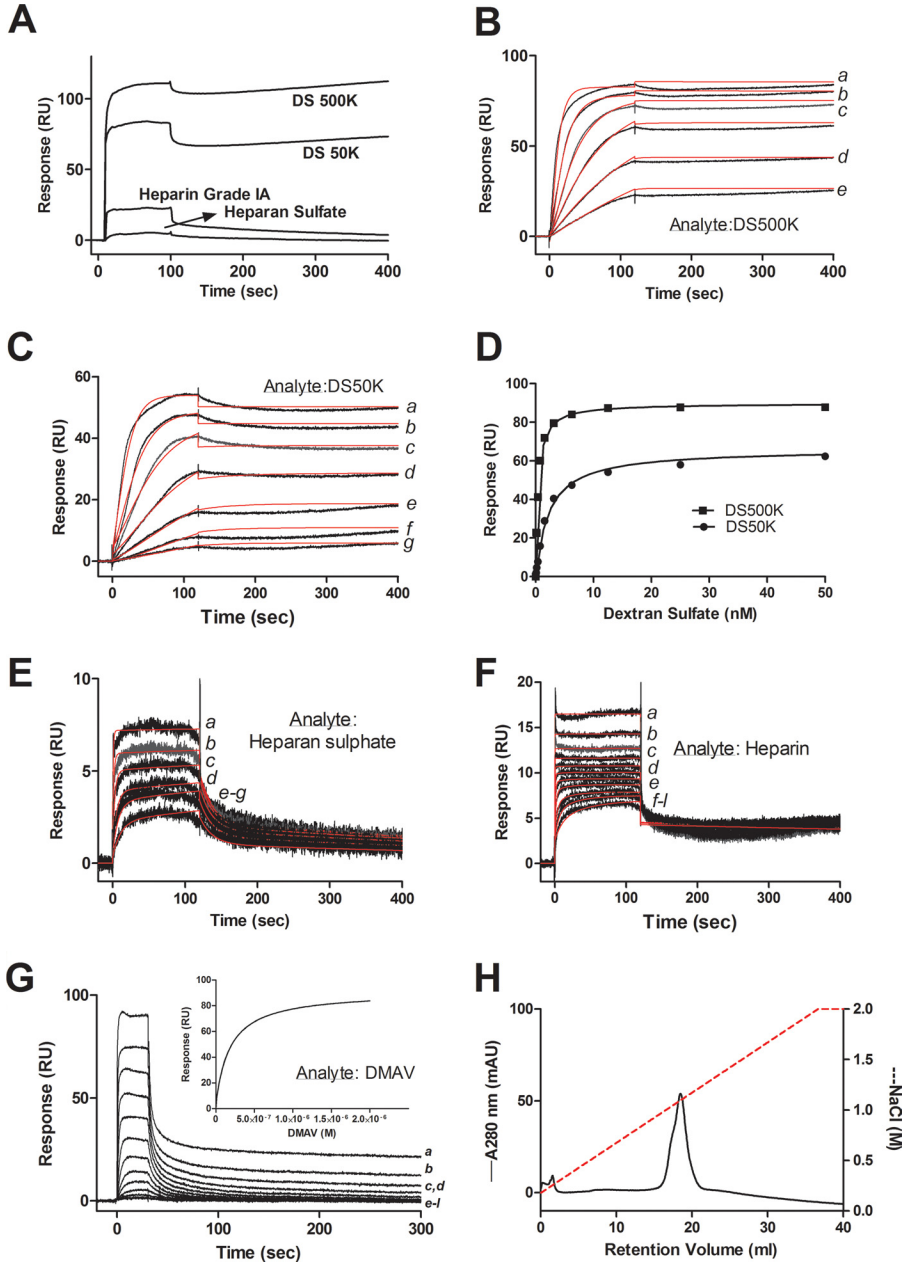

FIGURE 8. **DMAV interacts with sulfated glycans.** *A*, DMAV was immobilized in a CM5 sensor chip followed by injection of 200 nmol/liter DS500K or DS50K or heparin Grade I (40 μmol/liter) and heparan sulfate (4 μmol/liter). No signal was observed for 200 nmol/liter of chondroitin sulfate, dextran standard of 12,000 Da (non-sulfated), and dextran (non-sulfated) standard of 670,000 Da. All analytes were diluted in HBS-P. *B*, kinetics of DS500K interaction with immobilized DMAV. DS500K was injected for 120 s for association phase and 600 s for dissociation phase. Concentrations were 6.25 nmol/liter (*a*), 3.125 nmol/liter (*b*), 1.56 nmol/liter (*c*), 0.78 nmol/liter (*d*), and 0.39 nmol/liter (*e*). The fitting using a bivalent ligand model is shown in *red*. *C*, kinetics of DS50K interaction with immobilized DMAV. DS50K was injected for 120 s for association phase and 600 s for dissociation phase. Concentrations of DS50K were 12.5 nmol/liter (*a*), 6.25 nmol/liter (*b*), 3.125 nmol/liter (*c*), 1.56 nmol/liter (*d*), 0.78 nmol/liter (*e*), 0.39 nmol/liter (*f*), and 0.19 nmol/liter (*g*). The fitting using a bivalent ligand model is shown in *red*. *D*, steady-state kinetics for DS50K and DS500K interaction with immobilized DMAV determined a K_D of 0.46 nmol/liter (DS500K) and 1.97 nmol/liter (DS50K). *E*, kinetics of the interaction of heparan sulfate with immobilized DMAV. Heparan sulfate concentrations were 100 μmol/liter (*a*), 50 μmol/liter (*b*), 25 μmol/liter (*c*), 12.5 μmol/liter (*d*), 6.25 μmol/liter (*e*), and 3.125 μmol/liter (*f*). Results were fitted with a two-state reaction model. *F*, kinetics of the interaction of heparin with immobilized DMAV. Heparin concentrations were 25 μmol/liter (*a*), 12.5 μmol/liter (*b*), 6.25 μmol/liter (*c*), 3.12 μmol/liter (*d*), 1.56 μmol/liter (*e*), 0.78 μmol/liter (*f*), 0.39 μmol/liter (*g*), 0.19 μmol/liter (*h*), 0.09 μmol/liter (*i*), 0.04 μmol/liter (*j*), and 0.02 μmol/liter (*k*). Results were fitted with a bivalent analyte model. *G*, kinetics of the interaction of DMAV with immobilized biotinylated heparin. DMAV concentrations were 2000 nmol/liter (*a*), 1000 nmol/liter (*b*), 500 nmol/liter (*c*), 250 nmol/liter (*d*), 125 nmol/liter (*e*), 62.5 nmol/liter (*f*), 31.25 nmol/liter (*g*), 15.6 nmol/liter (*h*), 7.8 nmol/liter (*i*), 3.9 nmol/liter (*j*), 1.9 nmol/liter (*k*), and *l*, 0.9 nmol/liter (*l*). *Inset*, steady-state kinetics yield a K_D of 97 nmol/liter. *H*, DMAV interacts with a heparin-agarose column. DMAV (200 μl; 10 μmol/liter) was added onto the heparin column and equilibrated in Tris (20 mmol/liter), NaCl (0.15 mol/liter), pH 7.4. After washing the column, a gradient (NaCl, 0–2 mol/liter) was applied for 40 min. The peak corresponding to DMAV eluted at ~1 mol/liter NaCl. *mAU*, milliabsorbance units.

sional SDS-PAGE followed by gel-tryptic digestion and MS/MS of the bands. Fig. 9, *F* (for fraction 21) and *G* (for fraction 23), shows that DMAV was identified without ambiguity as one of the most abundant components in addition to lipocalins. Fractions 21 and 23 were also evaluated for the Cu^{2+} content by ICP-MS. Fig. 9*H* demonstrates that Cu^{2+} is

detectable in fraction 21, and higher levels are observed in fraction 23. Finally, fractions 21 and 23 exhibit antioxidant activity using the cyt *c* reduction assay, which was metal-dependent because it was blocked by EDTA (Fig. 9*I*).

DISCUSSION

Studying the function of the antigen-5 family of proteins revealed that members of this family exhibit antioxidant activity. This was concluded based on several enzymatic or cell-

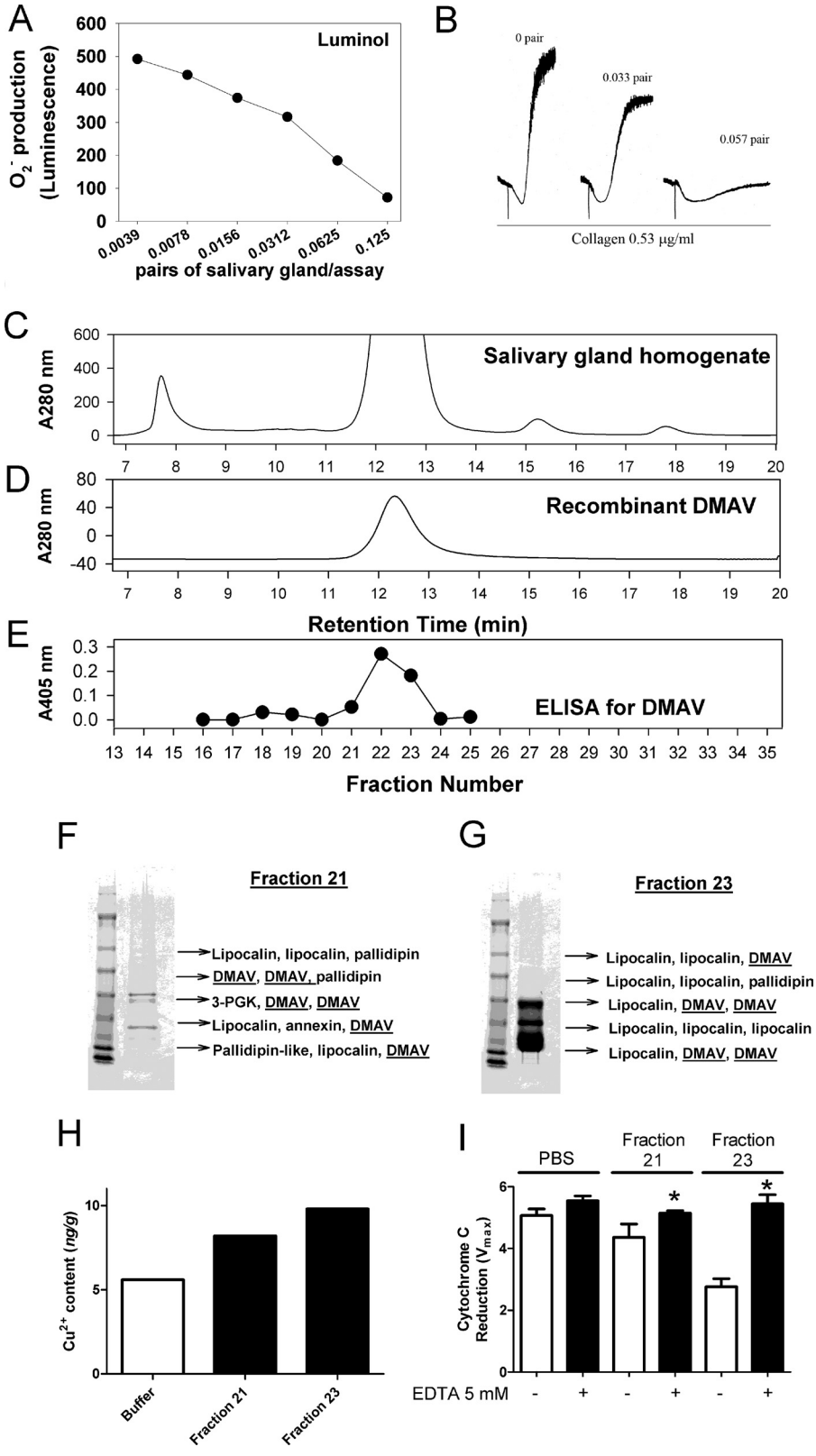

based assays. Accordingly, recombinant DMAV was found to scavenge $O_2^{\cdot-}$ produced by neutrophil activated by PMA and detected by two chemically unrelated luminescence reagents that react with $O_2^{\cdot-}$ (*e.g.* Diogenes reagent and lucigenin). DMAV also inhibits luminescence generated by luminol or the reduction of cyt *c* by $O_2^{\cdot-}$ generated in the X/XO system. Because DMAV does not block uric acid activity or consumption of oxygen after the addition of X/XO, it was evident that this molecule exhibits direct antioxidant properties through removal of $O_2^{\cdot-}$. In addition, the antioxidant activity of DMAV is specific for this molecule, because it was not found for several other salivary proteins expressed in *E. coli* or in insect cells.

Control experiments excluded the possibility that free thiols (41) or methionine oxidation (40) mediates the antioxidant function of DMAV. In contrast, EDTA completely abolished its antioxidant function, indicating a metal-dependent mechanism. ICP-MS was used to determine the metal content in DMAV. Results revealed that DMAV binds divalent ions Mn^{2+}, Co^{2+}, Ni^{2+}, Cu^{2+}, and Zn^{2+}. Through competition and displacement studies, it was concluded that DMAV has higher specificity for Cu^{2+} over other metals. Moreover, the addition of Cu^{2+} to apo-DMAV decreased the intrinsic fluorescence of the protein, indicating a conformational change upon binding. This experiment estimated an apparent K_D in the micromolar range, which is an overestimation because it is of the same order of magnitude as the protein concentration used in the assay. Under identical experimental conditions, Li_2SO_4 did not induce protein intrinsic fluorescence change. Furthermore, $CuSO_4$ does not induce intrinsic fluorescence change in DM146, an unrelated recombinant salivary protein.

Kinetic studies using a cytochrome *c* reduction assay suggest that Cu^{2+}-DMAV operates as a catalyst and not as a simple scavenger of $O_2^{\cdot-}$ (33, 45). Our interpretation is that antigen-5 members belong to a novel family of metal-dependent antioxidant enzymes. Of note, identification of Cu^{2+} as a ligand for DMAV is congruent with the identification of metal (*i.e.* Zn^{2+}) coordination in the structure of antigen-5 members from hookworm and snake venoms (50, 51). However, it remains to be determined how DMAV interacts with Cu^{2+} and the mechanism of metalation. The finding that Cu^{2+} preferentially binds to DMAV is also particularly relevant because Zn^{2+} does not exhibit redox potential and therefore cannot confer antioxidant properties to a protein. Structural information will be critical to gain further insight on the mechanism of action of DMAV.

With respect to metal requirements for antioxidant activity, Cu^{2+}-DMAV resembles Cu,Zn-SOD, which binds Cu^{2+} and also exhibits one of the highest k_{cat} values (k_{cat} for $O_2^{\cdot-}$, $\sim 2–3 \times 10^9$ mol liter^{-1} s^{-1}) (39, 45, 47). It has also been shown that several Cu^{2+} salts or low molar mass Cu^{2+} chelates exhibit a high catalytic redox potential and scavenge $O_2^{\cdot-}$ with efficiency close to that of Cu,Zn-SOD (52–55). Cu^{2+}-binding proteins, such as ceruloplasmin (56), prion protein PrP (57), and HAH1 (58), also display antioxidant activity. It is conceivable that DMAV employs an extremely efficient antioxidant mechanism for removal of $O_2^{\cdot-}$ that takes advantage of the high catalytic redox potential of Cu^{2+} (K_{cat} for $O_2^{\cdot-}$, $0.2–2 \times 10^9$ mol liter^{-1} s^{-1}), which is 1000 times higher than that for Mn^{2+} (K_{cat} for $O_2^{\cdot-}$, $1.3–8.9 \times 10^6$ mol liter^{-1} s^{-1}) (59, 60). It is important to recognize that Cu^{2+} binding molecules do not always behave as antioxidants. For example, Cu^{2+}-bound amyloid β peptide from Alzheimer disease (61) and α-synuclein-Cu^{2+} (62), or hydroquinone-Cu^{2+} complexes (63) are considered pro-oxidants, because they promote H_2O_2 formation without scavenging $O_2^{\cdot-}$. Accordingly, the pro- or antioxidant activity of Cu^{2+} in a protein complex is dependent on the number of Cu^{2+} per molecule, the redox state of Cu^{2+}, and the specific residues that coordinate the interaction with the metal (64–66).

Cu,Zn-SOD and Cu^{2+}-DMAV differ in several respects. On a molar basis, Cu^{2+}-DMAV is about 30–50 times less active than Cu,Zn-SOD. EDTA abolishes the antioxidant activity of Cu^{2+}-DMAV and other complexes (52, 53), but not Cu,Zn-SOD. This indicates that the interaction of DMAV with Cu^{2+} is not tight as observed with Cu,Zn-SOD (42, 45), as confirmed experimentally (Fig. 6*B*). Moreover, we did not detect accumulation of H_2O_2 production in the presence of DMAV. It is concluded that the products of spontaneous dismutation are identical to the products of the DMAV-catalyzed reaction, as initially reported for Cu,Zn-SOD (48). Furthermore, the Cu^{2+}-binding proteins such as tyrosinase, laccase, ascorbate oxidase (66), and, most notably, ceruloplasmin, scavenge $O_2^{\cdot-}$ but do not produce H_2O_2 (56, 67). It has been suggested that dismutation of $O_2^{\cdot-}$ by these proteins occurs through mechanisms that result in the production of water instead of H_2O_2 (66), although the chemistry of such dismutation is not completely understood (64–66). It is possible that DMAV might operate in a similar fashion.

Functionally, the antioxidant activity of DMAV or TIAV, which was characterized here as scavenging of $O_2^{\cdot-}$ *in vitro*, is consistent with inhibition of low doses of collagen-induced platelet aggregation, ATP secretion, and TXA_2 production. Indeed, Krotz *et al.* (10) and Caccese *et al.* (11) found that collagen, but not ADP or thrombin, is the only agonist that increases $O_2^{\cdot-}$ extracellularly. $O_2^{\cdot-}$ released by platelets also mediates platelet recruitment, by a mechanism inhibited by Cu,Zn-SOD (10). Furthermore, extracellular antioxidant *N*-acetylcysteine inhibits aggregation by low doses of collagen only and

FIGURE 9. **Dipetalogaster maxima salivary gland; effects on platelets, antioxidant activity, and Cu^{2+} content.** *A*, $O_2^{\cdot-}$ was generated by the X (500 μmol/liter)/XO (1.2 milliunits/ml) in the presence of SGH of *D. maxima*. Superoxide was detected by chemiluminescence using luminol. *B*, effects on platelet aggregation. Platelets were incubated with the SGH of *D. maxima* followed by the addition of collagen (0.53 μg/ml). Aggregation was detected by turbidimetry in a Lumi-Aggregometer. *C*, fractionation of the SG of *D. maxima*. SGH corresponding to 100 pairs of *D. maxima* was applied to a Sephadex-G75 column as eluted with PBS, pH 7.4, at a flow rate of 0.5 ml/min. *D*, recombinant DMAV (100 μg) was loaded into a Sephadex G-75 column equilibrated in PBS and eluted at 0.5 ml/min. *E*, ELISA for DMAV. Fifty μl of each fraction collected in *C* was added to Immulon 2HB plates, followed by incubation of anti-DMAV polyclonal antibodies and alkaline anti-rabbit phosphatase-coupled secondary antibodies as described under "Experimental Procedures." Fraction 21 (*F*) and fraction 23 (*G*) were separated by one-dimensional NuPAGE, and the bands were used for in-gel tryptic digestion and MS. Each peptide mass was searched against a database for the SG proteins from *D. maxima*. Results are indicated by *arrows*. *3-PGK*, 3-phosphoglycerol kinase. *H*, Cu^{2+} content of fractions 21 and 23 was estimated by ICP-MS. Expanded uncertainty of the *bars* are 50% of the value. *I*, antioxidant activity. Fractions 21 and 23 were tested for inhibition of cytochrome *c* reduction using X (500 μmol/liter)/XO (1.2 milliunits/ml) with and without EDTA (5 mmol/liter). Significance (*) was set at $p < 0.05$ (Student's *t* test). *Error bars*, S.E.

suppresses production of TXA_2 (12). In support of our findings that DMAV inhibits extracellular O_2^- is the result presented in Fig. 3*B* showing that Cu,Zn-SOD inhibits platelet aggregation by low doses of collagen only, but, as reported before, it does not interfere with aggregation induced by high concentrations, such as 6 μg/ml (10). Furthermore, the increase in extracellular O_2^- levels occurs after 2 min of collagen addition and coincides with the appearance of large aggregates (8). Our results demonstrated that the anti-aggregatory effect of DMAV is only observable at later time points (no effects in shape change), when the production of O_2^- has already started. Also, thrombus formation under flow in a collagen surface is only partially attenuated by negative modulators of intracellular O_2^- production, such as NADPH oxidase inhibitors (*e.g.* diphenylene iodonium, apocyanin, and 2-acetylphenothiazine) or Cu,Zn-SOD mimetic (*e.g.* MnTMPyP) (38, 68). In agreement with these results, TIAV, which acts extracellularly, marginally affected thrombus formation *in vitro* (Fig. 3*F*).

It is important to emphasize that although convulxin (Cvx) generates intracellular ROS (24, 69), it does not promote ROS increase extracellularly; nor does Cu,Zn-SOD inhibit platelet activation by Cvx (69). These results are therefore in agreement with the lack of effects of DMAV in aggregation caused by low doses of Cvx (Fig. 2*A*). Actually, this result is not surprising, because Cvx is a strong agonist that promotes direct PLCγ2 activation and that relies only marginally on secondary mediators (*e.g.* TXA_2 and ADP) to induce full platelet aggregation (70–72). Although thrombin or thrombin-receptor activating peptide (TRAP) induce ROS production intracellularly (38, 69) and aggregation is negatively modulated by intracellular antioxidants MnTMPyP (20) or Tempol (73), extracellular O_2^- in the supernatant of thrombin-activated platelets has not been detected by Krotz *et al.* (10) or Caccese *et al.* (11). Plausibly, this explains why DMAV does not affect thrombin-induced platelet aggregation (Fig. 2*A*). Finally, our experiments using ITC and platelet aggregation assays excluded the possibility that pro-aggregatory molecules involved in platelet aggregation by collagen, such as ADP or TXA_2, PGG_2/PGH_2, and 12-HETE (37), are targets for DMAV. It is concluded that DMAV interrupts platelet aggregation by a mechanism never reported before for a salivary protein that is explained by scavenging O_2^-. DMAV also attenuates the O_2^- signal generated by PMA-activated neutrophils, validating the view that different sources of ROS production are effectively blocked by the inhibitor.

Removal of O_2^- is particularly important because it is the limiting step in the generation of other ROS (*e.g.* hydroxyl and peroxyl). Although several reports have demonstrated a pivotal role for intracellular O_2^- as a signaling molecule and inflammatory mediator (74–77), extracellularly O_2^- also plays an important role in inflammation, as evidenced by the inhibitory role of extracellular SOD (EC-SOD or SOD3) in neutrophilic inflammation in the lung and in the skin (78–83). Conceivably, DMAV interferes with the proinflammatory effects of extracellular ROS produced by neutrophils, platelets, and other cell types (84, 85), resulting in attenuation of expression of procoagulant tissue factor, NET formation, cytokine release, lipid peroxidation, and conversion of nitric oxide to peroxynitrite in the vasculature (86–90). In other words, scavenging of extracellular O_2^- down-modulates a myriad of proinflammatory reactions.

SPR results and affinity chromatography experiments demonstrated that DMAV interacts with immobilized heparin (K_D ~100 nmol/liter) and other sulfated compounds (*e.g.* heparan sulfate and dextran sulfate). This finding reveals a remarkable similarity of DMAV with extracellular Cu,Zn-SOD, which binds heparin sulfate proteoglycans on cell surfaces via its heparin-binding domain (86). It is conceivable that binding of DMAV to endothelial cells increases the effective concentration of the enzyme and the antioxidant tonus at bite sites. Further, the presence of DMAV in the salivary gland was supported by the identification of metal-dependent antioxidant activity in chromatographic fractions containing native DMAV, confirmed by mass spectrometry and ELISA. Nevertheless, purification of native DMAV from the gland will be necessary in order to fully characterize it as an enzyme in nature, through the determination of the metal content and the kinetics and products of the reaction with O_2^-. Finally, it is notable that the salivary glands of blood-sucking arthropods reportedly contain at least one antiplatelet, one anticoagulant, and one vasodilator (1). Based on the results presented herein, and because antigen-5 members are ubiquitously found and relatively abundant, it is fair to say that at least one antioxidant might also be present in these glands.

The discovery of novel protein families in insect salivary protein or other exogenous secretions has proven particularly important in our understanding of vertebrate vascular biology and in providing tools for biochemistry and cell biology or to predict the function of endogenous proteins (1, 2). By analogy with DMAV, we speculate that other endogenous CAP/antigen-5 members (*e.g.* GLIPR1, GAPRI, PI15, and CRISP) (26) might also behave as metal-binding proteins with pro- or antioxidant functions. In conclusion, expression of antigen-5 members in the SGs of insects and ticks counteracts the diverse proinflammatory function of O_2^- in the microcirculation, contributing to the successful feeding of blood-sucking arthropods.

Acknowledgments—We are thankful to Ming Zheng, Renee Olano, and Carl Hammer (NIAID, National Institutes of Health, Research Technology Branch) for mass spectrometry analysis. We thank Dr. J. L. Villeval (Institut National de la Santé et de la Recherche Médicale (INSERM), Paris, France) for providing recombinant GPVI and Dr. Murali Krishna (NCI/NIH) for discussions and expertise with the Clark electrode. We are grateful to Brenda Rae Marshall (Division of Intramural Research Program Support Staff, NIAID, National Institutes of Health) for editing.

REFERENCES

1. Ribeiro, J. M., and Francischetti, I. M. (2003) Role of arthropod saliva in blood feeding. Sialome and post-sialome perspectives. *Annu. Rev. Entomol.* **48,** 73–88
2. Francischetti, I. M. (2010) Platelet aggregation inhibitors from hematophagous animals. *Toxicon* **56,** 1130–1144
3. Mans, B. J., Francischetti, I. M. (2010) Sialomic perspectives on the evolution of blood-feeding behavior in arthropods. Future therapeutics by natural design. *Toxins and Hemostasis: From bench to Bedside* (Kini, R. M., Clemetson, K. J., Markland, F. S., McLane, M. A., and Morita, T., eds) pp.

21–44, Springer, New York
4. Ma, D., Xu, X., An, S., Liu, H., Yang, X., Andersen, J. F., Wang, Y., Tokumasu, F., Ribeiro, J. M., Francischetti, I. M., and Lai, R. (2011) A novel family of RGD-containing disintegrins (Tablysin-15) from the salivary gland of the horsefly *Tabanus yao* targets αIIbβ3 or αVβ3 and inhibits platelet aggregation and angiogenesis. *Thromb. Haemost.* **105,** 1032–1045
5. Xu, X., Francischetti, I. M., Lai, R., Ribeiro, J. M., and Andersen, J. F. (2012) Structure of protein having inhibitory disintegrin and leukotriene scavenging functions contained in a single domain. *J. Biol. Chem.* **287,** 10967–10976
6. Assumpcão, T. C., Charneau, S., Santiago, P. B., Francischetti, I. M., Meng, Z., Araújo, C. N., Pham, V. M., Queiroz, R. M., de Castro, C. N., Ricart, C. A., Santana, J. M., and Ribeiro, J. M. (2011) Insight into the salivary transcriptome and proteome of *Dipetalogaster maxima*. *J. Proteome Res.* **10,** 669–679
7. Assumpção, T. C., Francischetti, I. M., Andersen, J. F., Schwarz, A., Santana, J. M., and Ribeiro, J. M. (2008) An insight into the sialome of the blood-sucking bug *Triatoma infestans*, a vector of Chagas' disease. *Insect Biochem. Mol. Biol.* **38,** 213–232
8. Krötz, F., Sohn, H. Y., and Pohl, U. (2004) Reactive oxygen species. Players in the platelet game. *Arterioscler. Thromb. Vasc. Biol.* **24,** 1988–1996
9. Arthur, J. F., Gardiner, E. E., Kenny, D., Andrews, R. K., and Berndt, M. C. (2008) Platelet receptor redox regulation. *Platelets* **19,** 1–8
10. Krötz, F., Sohn, H. Y., Gloe, T., Zahler, S., Riexinger, T., Schiele, T. M., Becker, B. F., Theisen, K., Klauss, V., and Pohl, U. (2002) NAD(P)H oxidase-dependent platelet superoxide anion release increases platelet recruitment. *Blood* **100,** 917–924
11. Caccese, D., Praticò, D., Ghiselli, A., Natoli, S., Pignatelli, P., Sanguigni, V., Iuliano, L., and Violi, F. (2000) Superoxide anion and hydroxyl radical release by collagen-induced platelet aggregation. Role of arachidonic acid metabolism. *Thromb. Haemost.* **83,** 485–490
12. Tang, W. H., Stitham, J., Gleim, S., Di Febbo, C., Porreca, E., Fava, C., Tacconelli, S., Capone, M., Evangelista, V., Levantesi, G., Wen, L., Martin, K., Minuz, P., Rade, J., Patrignani, P., and Hwa, J. (2011) Glucose and collagen regulate human platelet activity through aldose reductase induction of thromboxane. *J. Clin. Invest.* **121,** 4462–4476
13. Leo, R., Praticò, D., Iuliano, L., Pulcinelli, F. M., Ghiselli, A., Pignatelli, P., Colavita, A. R., FitzGerald, G. A., and Violi, F. (1997) Platelet activation by superoxide anion and hydroxyl radicals intrinsically generated by platelets that had undergone anoxia and then reoxygenated. *Circulation* **95,** 885–891
14. Salvemini, D., de Nucci, G., Sneddon, J. M., and Vane, J. R. (1989) Superoxide anions enhance platelet adhesion and aggregation. *Br. J. Pharmacol.* **97,** 1145–1150
15. Yao, S. K., Ober, J. C., Gonenne, A., Clubb, F. J., Jr., Krishnaswami, A., Ferguson, J. J., Anderson, H. V., Gorecki, M., Buja, L. M., and Willerson, J. T. (1993) Active oxygen species play a role in mediating platelet aggregation and cyclic flow variations in severely stenosed and endothelium-injured coronary arteries. *Circ. Res.* **73,** 952–967
16. Pignatelli, P., Pulcinelli, F. M., Lenti, L., Gazzaniga, P. P., and Violi, F. (1998) Hydrogen peroxide is involved in collagen-induced platelet activation. *Blood* **91,** 484–490
17. Iuliano, L., Colavita, A. R., Leo, R., Praticò, D., and Violi, F. (1997) Oxygen free radicals and platelet activation. *Free Radic. Biol. Med.* **22,** 999–1006
18. Praticò, D., Iuliano, L., Alessandri, C., Camastra, C., and Violi, F. (1993) Polymorphonuclear leukocyte-derived O_2-reactive species activate primed platelets in human whole blood. *Am. J. Physiol.* **264,** H1582–H1587
19. Pratico, D., Iuliano, L., Pulcinelli, F. M., Bonavita, M. S., Gazzaniga, P. P., and Violi, F. (1992) Hydrogen peroxide triggers activation of human platelets selectively exposed to nonaggregating concentrations of arachidonic acid and collagen. *J. Lab. Clin. Med.* **119,** 364–370
20. Chlopicki, S., Olszanecki, R., Janiszewski, M., Laurindo, F. R., Panz, T., and Miedzobrodzki, J. (2004) Functional role of NADPH oxidase in activation of platelets. *Antioxid. Redox Signal.* **6,** 691–698
21. Clemetson, K. J., and Clemetson, J. M. (2007) Collagen receptors as potential targets for novel anti-platelet agents. *Curr. Pharm. Des.* **13,** 2673–2683
22. Begonja, A. J., Teichmann, L., Geiger, J., Gambaryan, S., and Walter, U. (2006) Platelet regulation by NO/cGMP signaling and NAD(P)H oxidase-generated ROS. *Blood Cells Mol. Dis.* **36,** 166–170
23. Watson, S. P. (2009) Platelet activation by extracellular matrix proteins in haemostasis and thrombosis. *Curr. Pharm. Des.* **15,** 1358–1372
24. Arthur, J. F., Qiao, J., Shen, Y., Davis, A. K., Dunne, E., Berndt, M. C., Gardiner, E. E., and Andrews, R. K. (2012) ITAM receptor-mediated generation of reactive oxygen species in human platelets occurs via Syk-dependent and Syk-independent pathways. *J. Thromb. Haemost.* **10,** 1133–1141
25. Hubbard, G. P., Wolffram, S., Lovegrove, J. A., and Gibbins, J. M. (2004) Ingestion of quercetin inhibits platelet aggregation and essential components of the collagen-stimulated platelet activation pathway in humans. *J. Thromb. Haemost.* **2,** 2138–2145
26. Gibbs, G. M., Roelants, K., and O'Bryan, M. K. (2008) The CAP superfamily. Cysteine-rich secretory proteins, antigen 5, and pathogenesis-related 1 proteins. Roles in reproduction, cancer, and immune defense. *Endocr. Rev.* **29,** 865–897
27. Francischetti, I. M., Saliou, B., Leduc, M., Carlini, C. R., Hatmi, M., Randon, J., Faili, A., and Bon, C. (1997) Convulxin, a potent platelet-aggregating protein from *Crotalus durissus terrificus* venom, specifically binds to platelets. *Toxicon* **35,** 1217–1228
28. Jandrot-Perrus, M., Busfield, S., Lagrue, A. H., Xiong, X., Debili, N., Chickering, T., Le Couedic, J. P., Goodearl, A., Dussault, B., Fraser, C., Vainchenker, W., and Villeval, J. L. (2000) Cloning, characterization, and functional studies of human and mouse glycoprotein VI. A platelet-specific collagen receptor from the immunoglobulin superfamily. *Blood* **96,** 1798–1807
29. Francischetti, I. M., Assumpcao, T. C., Ma, D., Li, Y., Vicente, E. C., Uieda, W., and Ribeiro, J. M. (2013) The "Vampirome": transcriptome and proteome analysis of the principal and accessory submaxillary glands of the vampire bat *Desmodus rotundus,* a vector of human rabies. *J. Proteomics* **82,** 288–319
30. Assumpção, T. C., Alvarenga, P. H., Ribeiro, J. M., Andersen, J. F., and Francischetti, I. M. (2010) Dipetalodipin, a novel multifunctional salivary lipocalin that inhibits platelet aggregation, vasoconstriction, and angiogenesis through unique binding specificity for TXA2, PGF2α, and 15(*S*)-HETE. *J. Biol. Chem.* **285,** 39001–39012
31. Whitmore, L., and Wallace, B. A. (2004) DICHROWEB, an online server for protein secondary structure analyses from circular dichroism spectroscopic data. *Nucleic Acids Res.* **32,** W668–W673
32. Whitmore, L., and Wallace, B. A. (2008) Protein secondary structure analyses from circular dichroism spectroscopy. Methods and reference databases. *Biopolymers* **89,** 392–400
33. Krishna, M. C., Russo, A., Mitchell, J. B., Goldstein, S., Dafni, H., and Samuni, A. (1996) Do nitroxide antioxidants act as scavengers of $O_2^{\cdot-}$ or as SOD mimics? *J. Biol. Chem.* **271,** 26026–26031
34. Krishna, M. C., Samuni, A., Taira, J., Goldstein, S., Mitchell, J. B., and Russo, A. (1996) Stimulation by nitroxides of catalase-like activity of hemeproteins. Kinetics and mechanism. *J. Biol. Chem.* **271,** 26018–26025
35. Schultz, M. K., Biegalski, S. R., Inn, K. G., Yu, L., Burnett, W. C., Thomas, J. L., and Smith, G. E. (1999) Optimizing the removal of carbon phases in soils and sediments for sequential chemical extractions by coulometry. *J. Environ. Monit.* **1,** 183–190
36. Collin, N., Assumpção, T. C., Mizurini, D. M., Gilmore, D. C., Dutra-Oliveira, A., Kotsyfakis, M., Sá-Nunes, A., Teixeira, C., Ribeiro, J. M., Monteiro, R. Q., Valenzuela, J. G., and Francischetti, I. M. (2012) Lufaxin, a novel factor Xa inhibitor from the salivary gland of the sand fly *Lutzomyia longipalpis* blocks protease-activated receptor 2 activation and inhibits inflammation and thrombosis *in vivo*. *Arterioscler. Thromb. Vasc. Biol.* **32,** 2185–2198
37. Watson, S. P., Auger, J. M., McCarty, O. J., and Pearce, A. C. (2005) GPVI and integrin αIIb β3 signaling in platelets. *J. Thromb. Haemost.* **3,** 1752–1762
38. Begonja, A. J., Gambaryan, S., Geiger, J., Aktas, B., Pozgajova, M., Nieswandt, B., and Walter, U. (2005) Platelet NAD(P)H-oxidase-generated ROS production regulates αIIbβ3-integrin activation independent of the NO/cGMP pathway. *Blood* **106,** 2757–2760
39. Fridovich, I. (1995) Superoxide radical and superoxide dismutases. *Annu.*

Rev. Biochem. **64,** 97–112
40. Levine, R. L., Mosoni, L., Berlett, B. S., and Stadtman, E. R. (1996) Methionine residues as endogenous antioxidants in proteins. *Proc. Natl. Acad. Sci. U.S.A.* **93,** 15036–15040
41. Cox, A. G., Winterbourn, C. C., and Hampton, M. B. (2010) Mitochondrial peroxiredoxin involvement in antioxidant defence and redox signalling. *Biochem. J.* **425,** 313–325
42. Goto, J. J., Zhu, H., Sanchez, R. J., Nersissian, A., Gralla, E. B., Valentine, J. S., and Cabelli, D. E. (2000) Loss of *in vitro* metal ion binding specificity in mutant copper-zinc superoxide dismutases associated with familial amyotrophic lateral sclerosis. *J. Biol. Chem.* **275,** 1007–1014
43. Kosman, D. J. (2010) Multicopper oxidases. A workshop on copper coordination chemistry, electron transfer, and metallophysiology. *J. Biol. Inorg. Chem.* **15,** 15–28
44. Sakurai, T., and Kataoka, K. (2007) Structure and function of type I copper in multicopper oxidases. *Cell Mol. Life Sci.* **64,** 2642–2656
45. Goldstein, S., Fridovich, I., and Czapski, G. (2006) Kinetic properties of Cu,Zn-superoxide dismutase as a function of metal content. Order restored. *Free Radic. Biol. Med.* **41,** 937–941
46. Butler, J., Koppenol, W. H., and Margoliash, E. (1982) Kinetics and mechanism of the reduction of ferricytochrome *c* by the superoxide anion. *J. Biol. Chem.* **257,** 10747–10750
47. Klug, D., Rabani, J., and Fridovich, I. (1972) A direct demonstration of the catalytic action of superoxide dismutase through the use of pulse radiolysis. *J. Biol. Chem.* **247,** 4839–4842
48. McCord, J. M., and Fridovich, I. (1969) Superoxide dismutase. An enzymic function for erythrocuprein (hemocuprein). *J. Biol. Chem.* **244,** 6049–6055
49. Sandström, J., Carlsson, L., Marklund, S. L., and Edlund, T. (1992) The heparin-binding domain of extracellular superoxide dismutase C and formation of variants with reduced heparin affinity. *J. Biol. Chem.* **267,** 18205–18209
50. Asojo, O. A. (2011) Structure of a two-CAP-domain protein from the human hookworm parasite *Necator americanus*. *Acta Crystallogr. D Biol. Crystallogr.* **67,** 455–462
51. Wang, Y. L., Kuo, J. H., Lee, S. C., Liu, J. S., Hsieh, Y. C., Shih, Y. T., Chen, C. J., Chiu, J. J., and Wu, W. G. (2010) Cobra CRISP functions as an inflammatory modulator via a novel Zn^{2+}- and heparan sulfate-dependent transcriptional regulation of endothelial cell adhesion molecules. *J. Biol. Chem.* **285,** 37872–37883
52. Kubota, S., and Yang, J. T. (1984) Bis[cyclo(histidylhistidine)]copper(II) complex that mimics the active center of superoxide dismutase has its catalytic activity. *Proc. Natl. Acad. Sci. U.S.A.* **81,** 3283–3286
53. Weser, U., and Schubotz, L. M. (1981) Catalytic reaction of copper complexes with superoxide. *Agents Actions Suppl.* **8,** 103–120
54. Brigelius, R., Spöttl, R., Bors, W., Lengfelder, E., Saran, M., and Weser, U. (1974) Superoxide dismutase activity of low molecular weight Cu2 plus-chelates studied by pulse radiolysis. *FEBS Lett.* **47,** 72–75
55. Fielden, E. M., Roberts, P. B., Bray, R. C., Lowe, D. J., Mautner, G. N., Rotilio, G., and Calabrese, L. (1974) Mechanism of action of superoxide dismutase from pulse radiolysis and electron paramagnetic resonance. Evidence that only half the active sites function in catalysis. *Biochem. J.* **139,** 49–60
56. Goldstein, I. M., Kaplan, H. B., Edelson, H. S., and Weissmann, G. (1979) Ceruloplasmin. A scavenger of superoxide anion radicals. *J. Biol. Chem.* **254,** 4040–4045
57. Davies, P., and Brown, D. R. (2008) The chemistry of copper binding to PrP. Is there sufficient evidence to elucidate a role for copper in protein function? *Biochem. J.* **410,** 237–244
58. Hung, I. H., Casareno, R. L., Labesse, G., Mathews, F. S., and Gitlin, J. D. (1998) HAH1 is a copper-binding protein with distinct amino acid residues mediating copper homeostasis and antioxidant defense. *J. Biol. Chem.* **273,** 1749–1754
59. Barnese, K., Gralla, E. B., Cabelli, D. E., and Valentine, J. S. (2008) Manganous phosphate acts as a superoxide dismutase. *J. Am. Chem. Soc.* **130,** 4604–4606
60. Spasojević, I., Batinić-Haberle, I., Stevens, R. D., Hambright, P., Thorpe, A. N., Grodkowski, J., Neta, P., and Fridovich, I. (2001) Manganese(III) biliverdin IX dimethyl ester. A powerful catalytic scavenger of superoxide employing the Mn(III)/Mn(IV) redox couple. *Inorg. Chem.* **40,** 726–739
61. Huang, X., Atwood, C. S., Hartshorn, M. A., Multhaup, G., Goldstein, L. E., Scarpa, R. C., Cuajungco, M. P., Gray, D. N., Lim, J., Moir, R. D., Tanzi, R. E., and Bush, A. I. (1999) The Aβ peptide of Alzheimer's disease directly produces hydrogen peroxide through metal ion reduction. *Biochemistry* **38,** 7609–7616
62. Davies, P., Wang, X., Sarell, C. J., Drewett, A., Marken, F., Viles, J. H., and Brown, D. R. (2011) The synucleins are a family of redox-active copper binding proteins. *Biochemistry* **50,** 37–47
63. Li, Y., Kuppusamy, P., Zweier, J. L., and Trush, M. A. (1995) ESR evidence for the generation of reactive oxygen species from the copper-mediated oxidation of the benzene metabolite, hydroquinone. Role in DNA damage. *Chem. Biol. Interact.* **94,** 101–120
64. Bento, I., Silva, C. S., Chen, Z., Martins, L. O., Lindley, P. F., and Soares, C. M. (2010) Mechanisms underlying dioxygen reduction in laccases. Structural and modelling studies focusing on proton transfer. *BMC Struct. Biol.* **10,** 28
65. Gardner, R., Salvador, A., and Moradas-Ferreira, P. (2002) Why does SOD overexpression sometimes enhance, sometimes decrease, hydrogen peroxide production? A minimalist explanation. *Free Radic. Biol. Med.* **32,** 1351–1357
66. Frieden, E., Osaki, S., and Kobayashi, H. (1965) Copper proteins and oxygen. Correlations between structure and function of the copper oxidases. *J. Gen. Physiol.* **49,** (suppl.) 213–252
67. Marklund, S. L. (1986) Ceruloplasmin, extracellular-superoxide dismutase, and scavenging of superoxide anion radicals. *J. Free Radic. Biol. Med.* **2,** 255–260
68. Vara, D., Campanella, M., and Pula, G. (2013) The novel NOX inhibitor 2-acetylphenothiazine impairs collagen-dependent thrombus formation in a GPVI-dependent manner. *Br. J. Pharmacol.* **168,** 212–224
69. Bakdash, N., and Williams, M. S. (2008) Spatially distinct production of reactive oxygen species regulates platelet activation. *Free Radic. Biol. Med.* **45,** 158–166
70. Faili, A., Randon, J., Francischetti, I. M., Vargaftig, B. B., and Hatmi, M. (1994) Convulxin-induced platelet aggregation is accompanied by a powerful activation of the phospholipase C pathway. *Biochem. J.* **298**, 87–91
71. Francischetti, I. M., Ghazaleh, F. A., Reis, R. A., Carlini, C. R., and Guimarães, J. A. (1998) Convulxin induces platelet activation by a tyrosine-kinase-dependent pathway and stimulates tyrosine phosphorylation of platelet proteins, including PLCγ2, independently of integrin αIIb β3. *Arch. Biochem. Biophys.* **353,** 239–250
72. Vargaftig, B. B., Prado-Franceschi, J., Chignard, M., Lefort, J., and Marlas, G. (1980) Activation of guinea-pig platelets induced by convulxin, a substance extracted from the venom of *Crotalus durissus cascavella*. *Eur. J. Pharmacol.* **68,** 451–464
73. Clutton, P., Miermont, A., and Freedman, J. E. (2004) Regulation of endogenous reactive oxygen species in platelets can reverse aggregation. *Arterioscler. Thromb. Vasc. Biol.* **24,** 187–192
74. Widlansky, M. E., and Gutterman, D. D. (2011) Regulation of endothelial function by mitochondrial reactive oxygen species. *Antioxid. Redox. Signal.* **15,** 1517–1530
75. Murphy, E., and Steenbergen, C. (2008) Mechanisms underlying acute protection from cardiac ischemia-reperfusion injury. *Physiol. Rev.* **88,** 581–609
76. Leonarduzzi, G., Sottero, B., Testa, G., Biasi, F., and Poli, G. (2011) New insights into redox-modulated cell signaling. *Curr. Pharm. Des.* **17,** 3994–4006
77. Thomas, S. R., Witting, P. K., and Drummond, G. R. (2008) Redox control of endothelial function and dysfunction. Molecular mechanisms and therapeutic opportunities. *Antioxid. Redox Signal.* **10,** 1713–1765
78. Yasui, K., and Baba, A. (2006) Therapeutic potential of superoxide dismutase (SOD) for resolution of inflammation. *Inflamm. Res.* **55,** 359–363
79. Ueda, J., Starr, M. E., Takahashi, H., Du, J., Chang, L. Y., Crapo, J. D., Evers, B. M., and Saito, H. (2008) Decreased pulmonary extracellular superoxide dismutase during systemic inflammation. *Free Radic. Biol. Med.* **45,** 897–904
80. Hassett, P., Curley, G. F., Contreras, M., Masterson, C., Higgins, B. D., O'Brien, T., Devaney, J., O'Toole, D., and Laffey, J. G. (2011) Overex-

pression of pulmonary extracellular superoxide dismutase attenuates endotoxin-induced acute lung injury. *Intensive Care Med.* **37,** 1680–1687
81. Gao, F., Koenitzer, J. R., Tobolewski, J. M., Jiang, D., Liang, J., Noble, P. W., and Oury, T. D. (2008) Extracellular superoxide dismutase inhibits inflammation by preventing oxidative fragmentation of hyaluronan. *J. Biol. Chem.* **283,** 6058–6066
82. Bowler, R. P., Nicks, M., Tran, K., Tanner, G., Chang, L. Y., Young, S. K., and Worthen, G. S. (2004) Extracellular superoxide dismutase attenuates lipopolysaccharide-induced neutrophilic inflammation. *Am. J. Respir. Cell Mol. Biol.* **31,** 432–439
83. Lee, Y. S., Cheon, I. S., Kim, B. H., Kwon, M. J., Lee, H. W., and Kim, T. Y. (2013) Loss of extracellular superoxide dismutase induces severe IL-23-mediated skin inflammation in mice. *J. Invest. Dermatol.* **133,** 732–741
84. Grommes, J., and Soehnlein, O. (2011) Contribution of neutrophils to acute lung injury. *Mol. Med.* **17,** 293–307
85. Segel, G. B., Halterman, M. W., and Lichtman, M. A. (2011) The paradox of the neutrophil's role in tissue injury. *J. Leukoc. Biol.* **89,** 359–372
86. Faraci, F. M., and Didion, S. P. (2004) Vascular protection. Superoxide dismutase isoforms in the vessel wall. *Arterioscler. Thromb. Vasc. Biol.* **24,** 1367–1373
87. Batinić-Haberle, I., Rebouças, J. S., and Spasojević, I. (2010) Superoxide dismutase mimics: chemistry, pharmacology, and therapeutic potential. *Antioxid. Redox Signal.* **13,** 877–918
88. Jiang, F., Zhang, Y., and Dusting, G. J. (2011) NADPH oxidase-mediated redox signaling. Roles in cellular stress response, stress tolerance, and tissue repair. *Pharmacol. Rev.* **63,** 218–242
89. Phillipson, M., and Kubes, P. (2011) The neutrophil in vascular inflammation. *Nat. Med.* **17,** 1381–1390
90. Bedard, K., and Krause, K. H. (2007) The NOX family of ROS-generating NADPH oxidases. Physiology and pathophysiology. *Physiol. Rev.* **87,** 245–313